

AD-A169 300

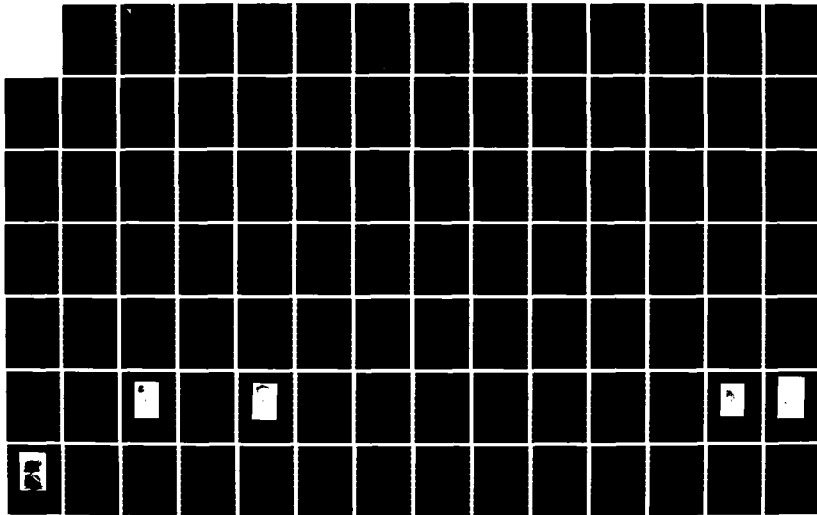
PULSED-LASER HIGH SPEED PHOTOGRAPHY OF ROCKET
PROPELLANT SURFACE DEFLAGRATION(U) DAYTON UNIV OH
RESEARCH INST R J BECKER MAY 86 UD-TR-85-147

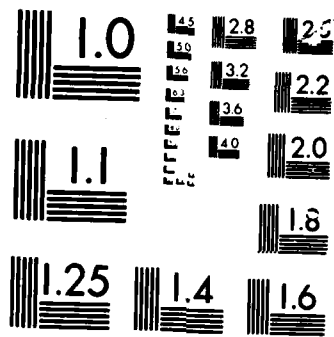
1/2

UNCLASSIFIED

AFRPL-TR-86-039 F04611-03-K-0023

F/G 21/9.2 NL





MICROCOPY

CHART

AD-A169 308

13



AFRPL TR-86-039

AD:

Final Report
for the period
1 May 1983 to
30 September 1985

Pulsed-Laser, High Speed Photography of Rocket Propellant Surface Deflagration

May 1986

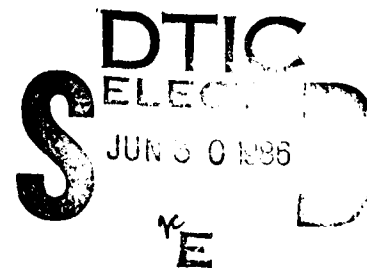
Author:
R. J. Becker

University of Dayton
Research Institute
Dayton, OH 45469-0001

UD-TR-85-147
F04611-83-K-0023

Approved for Public Release

Distribution is unlimited. The AFRPL Technical Services Office has reviewed this report, and it is releasable to the National Technical Information Service, where it will be available to the general public, including foreign nationals.



prepared for the:

**Air Force
Rocket Propulsion
Laboratory**

Air Force Space Technology Center
Space Division, Air Force Systems Command
Edwards Air Force Base,
California 93523-5000

DTIC FILE COPY

86 6 30 013

NOTICE

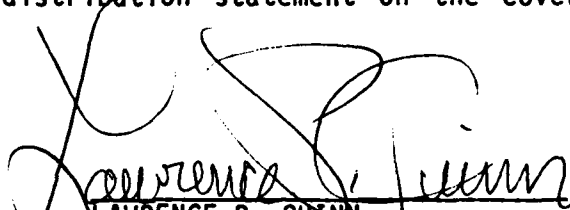
When U.S. Government drawings, specifications, or other data are used for any purpose other than a definitely related government procurement operation, the government thereby incurs no responsibility nor any obligation whatsoever, and the fact that the government may have formulated, furnished, or in any way supplied the said drawings, specifications, or other data, is not to be regarded by implication or otherwise, or conveying any rights or permission to manufacture, use, or sell any patented invention that may in any way be related thereto.

FOREWORD

This report was submitted by the University of Dayton Research Institute, Dayton, Ohio 45469 under Contract F04611-83-K-0023 with the Air Force Rocket Propulsion Laboratory (AFRPL). The report includes all work performed from 1 May 1983 to 30 September 1985. Research was performed at the University of Dayton Research Institute. Principal Investigator was Dr Roger J. Becker. AFRPL Project Manager was Mr Gary L. Vogt.

This technical report has been reviewed and is approved for publication and distribution in accordance with the distribution statement on the cover and on the DD Form 1473.


GARY L. VOGT
Project Manager


LAWRENCE P. QUINN
Chief, Aerothermochemistry
Branch

FOR THE DIRECTOR


DAVID L. NEURAUTER, Lt Col, USAF
Deputy Chief, Propulsion Analysis Division

REPORT DOCUMENTATION PAGE

1a. REPORT SECURITY CLASSIFICATION Unclassified		1b. RESTRICTIVE MARKINGS N/A	
2a. SECURITY CLASSIFICATION AUTHORITY N/A		3. DISTRIBUTION/AVAILABILITY OF REPORT Approved for public release; distribution is unlimited.	
2b. DECLASSIFICATION/DOWNGRADING SCHEDULE N/A			
4. PERFORMING ORGANIZATION REPORT NUMBER(S) UD-TR-85-147		5. MONITORING ORGANIZATION REPORT NUMBER(S) AFRPL-TR-86-039	
6a. NAME OF PERFORMING ORGANIZATION University of Dayton Research Institute	6b. OFFICE SYMBOL (If applicable)	7a. NAME OF MONITORING ORGANIZATION Air Force Rocket Propulsion Laboratory	
6c. ADDRESS (City, State and ZIP Code) University of Dayton Dayton, OH 45469-0001		7b. ADDRESS (City, State and ZIP Code) Edwards Air Force Base California 93523-5000	
8a. NAME OF FUNDING/SPONSORING ORGANIZATION	8b. OFFICE SYMBOL (If applicable)	9. PROCUREMENT INSTRUMENT IDENTIFICATION NUMBER F04611-83-K-0023	
3c. ADDRESS (City, State and ZIP Code)		10. SOURCE OF FUNDING NOS.	
		PROGRAM ELEMENT NO. 62302F	PROJECT NO. 5730
		TASK NO. 00	WORK UNIT NO. ER
11. TITLE (Include Security Classification) PULSED-LASER, HIGH-SPEED PHOTOGRAPHY OF ROCKET PROPELLANT SURFACE			
12. PERSONAL AUTHOR(S) Becker, Roger J.			
13a. TYPE OF REPORT Final	13b. TIME COVERED FROM 83/5/1 TO 85/9/30	14. DATE OF REPORT (Yr., Mo., Day) 86/5	15. PAGE COUNT 104
16. SUPPLEMENTARY NOTATION			
17. COSATI CODES		18. SUBJECT TERMS (Continue on reverse if necessary and identify by block number)	
FIELD	GROUP	SUB GR	Pulsed-Laser Photography, High-Speed Photography, Stereo Optics, Modulation Transfer Function, Optical Correlation, Deflagration.
21	09	2	
21	02		
19. ABSTRACT (Continue on reverse if necessary and identify by block number)			
<p>High-speed movies of solid propellant deflagration have long provided useful qualitative information on propellant behavior. Consequently, an extension of performance to include quantitative behavior of the surface, particularly the spatial relationship of particles across the surface, the temporal behavior of particles through extended periods of time, and accurate measurements of particle sizes, is highly desirable. Such measurements require the ability to take detailed movies across an extensive surface through the propellant flame for longer periods than the residence time of a given particle. For such experiments, camera optics employing magnification are undesirable, since they severely limit both the field-of-view and the depth-of-field, and hence, the useful duration of a frame sequence. Unfortunately, high resolution without magnification pushes both the diffraction limits and the performance capabilities</p> <p>(see reverse side)</p>			
20. DISTRIBUTION/AVAILABILITY OF ABSTRACT UNCLASSIFIED/UNLIMITED <input checked="" type="checkbox"/> SAME AS RPT <input type="checkbox"/> DTIC USERS <input type="checkbox"/>		21. ABSTRACT SECURITY CLASSIFICATION Unclassified	
22a. NAME OF RESPONSIBLE INDIVIDUAL Gary L. Vogt		22b. TELEPHONE NUMBER (Include Area Code) (805) 277-5258	22c. OFFICE SYMBOL AFRPL/DYCR

Box 11 (Continued)

DEFLAGRATION (U)

Box 19 (Continued)

of standard lenses. At this limit, the modulation transfer function (MTF) of the camera optics and film will greatly affect performance. The MTF of the optics can be improved by a factor of two or more at practical spatial frequencies by the use of monochromatic light, such as the reflected light from a laser. This is especially true for off-axis rays, an important consideration when an extended field-of-view is required. The use of an intense, short-pulsed laser has the additional advantage of suppressing flame brightness and motion blur. Such a light source must retain a high repetition rate to follow temporal behavior in detail.

High resolution at unity magnification is achieved by the use of 1.4 mJ of illumination energy per pulse in conjunction with a fine-grain film. This approach has worked well on both aluminized and pure aluminum perchlorate propellants. Since the pulses provide enough light to expose fine-grain film at unity magnification, it is possible to encompass an entire $\frac{1}{4}$ -inch strand surface in our field-of-view. Motion blur at 7 kHz framing rates and unity magnification is negligible ($1 \mu\text{m}$) due to the 25 ns width of the laser pulses. The short pulse width is also helpful in circumventing flame turbulence.

The quantitative analysis of the data provided by a photograph of an entire 6-mm-x-9-mm strand surface, containing from 7×10^4 to 10^5 pixels, is a demanding task. Economical results of satisfactory accuracy can be obtained using optical data processing. Preliminary conclusions from movies made using a copper-vapor laser as a light source and an optical correlator are presented. Movies were taken across the burning surfaces of $\frac{1}{4}$ -inch strands cut at oblique angles with resolutions of 25 microns for periods of 0.2-0.5 seconds. The optical correlator has worked well in providing temporal and spatial correlations. Attainment of quantitative statistical data using this correlator requires full-field information of the type obtained in the reported movies.

TABLE OF CONTENTS

SECTION		PAGE
1	Introduction	1
	1.1 Air Force Needs	1
	1.2 Limitations of Conventional Techniques	3
	1.3 Approach	5
	1.4 Scope	5
2	Experimental Discussion	8
	2.1 Hardware	8
	2.2 Optical System	14
	2.2.1 Physical Limits	14
	2.2.2 Optics	22
	2.3 Servopositioning Circuit	24
	2.3.1 Opto-Mechanical Subsystems	26
	2.3.2 Control Circuitry	31
	2.3.3 Servoperformance	38
	2.3.4 Local Burning Rate	39
	2.4 Laser Development and Synchronization Electronics	42
	2.4.1 Pulse Synchronization Circuit	42
	2.4.2 Copper-Vapor Laser Development	45
	2.5 Ancillary Work	47
	2.5.1 Film Development	47
	2.5.2 Inhibitor Development	49
	2.6 Optical Correlator	54
	2.6.1 Concept	55
	2.6.2 Practical Considerations and Limitations	58
	2.7 Stereo Cinephotography	60
3	Results	74
	3.1 General Performance	74
	3.2 AP Matrix Behavior	76
	3.3 Correlator Results	79
	3.4 Additional Observations	85
4	Conclusions	88
5	References	91

iii

Accession For	
NTIS GAI	<input checked="" type="checkbox"/>
DTIC TAB	<input type="checkbox"/>
Unannounced	<input type="checkbox"/>
Justification	<input type="checkbox"/>
By _____	
Distribution/	
Availability Codes	
Dist	Special
A-1	



LIST OF ILLUSTRATIONS

FIGURE		PAGE
1	Cross Section of Window Bomb.	9
2	Top View of Window Bomb.	10
3	Reentrant Window Port.	11
4	Modulation Transfer Function of Typical Single-Element Lens.	18
5	Modulation Transfer Function (MTF) of Film.	20
6	Modulation Transfer Function of White Light Vs. Monochromatic Light.	21
7	Modulation Transfer Function vs. Field-of-View.	23
8	Coherence Spoiler.	25
9	Mechanical Drive for Positional Controller.	27
10	Servooptics.	28
11	Diode-Array Control Circuit.	30
12	Detector and Analog Conditioning Circuit.	32
13	Digital Processing Circuit.	33
14	Analog Control Circuit.	34
15	Eight-Element Circuit Prototype.	37
16	Photodiode Array Trace Showing Surface Location vs. Time.	41
17	Pulse Synchronization Block Diagram.	43
18	Qualitative Performance of Commonly Used Inhibitors for Strand Experiments.	51
19	Chemical Structure of Phenolic Resin Copolymer Unit.	52
20	Qualitative Behavior of Polymer Inhibitor vs. Solution Concentration.	53
21	Optical Correlator.	59

LIST OF ILLUSTRATIONS
(Continued)

FIGURE		PAGE
22	Untreated Photograph of Combusting Surface.	61
23	Correlation Function Obtained from Untreated Photograph.	62
24	High-Contrast Photograph of Combusting Surface.	63
25	Correlation Function Obtained From a High-Contrast Photograph.	64
26	Top View of Port Design for Window Bomb.	66
27	Stereo Optics.	68
28	Side View of Window Bomb.	69
29	Stereo Images of Burning Propellant Surface.	71
30	Stereo Images of Burning Propellant Surface.	72
31	Stereo Images of Same Subject as Shown in Figure 29, Taken Several Frames Later.	73
32	Best Fit to Correlation-Width Data.	78
33	Exponential Fit to Size vs. Pressure Data.	81
34	Quadratic Fit to Size vs. Pressure Data.	82
35	Time Dependence of Correlation Peak Height.	84
36	Width of Cross-Correlation Functions vs. Separation in Time.	86

NOMENCLATURE

A	Adjustable parameter
b	Resolution of camera optics
b_1	Adjustable parameter
b_2	Adjustable parameter
B	Adjustable parameter
C	Adjustable parameter
D	Diameter of camera lens
f	Focal length of camera lens
f#	f-number = f/D
$f(t)$	Functional form of theoretical curve fitting measured correlation peak heights versus time
$f(p)$	Functional form of theoretical curve for correlation width versus pressure
$f(x,y)$	Transmittance of first image
$h(x,y)$	Transmittance of second image
I	Signal intensity
k_c	Cut-off spatial frequency of camera optics
k_1	Effective cut-off spatial frequency
m	Intensity modulation of an image
m_1	Adjustable parameter
m_2	Adjustable parameter
M	Magnification of camera optics
p	Pressure
x	Horizontal image coordinate
x_0	Amount of translation of an image in the x direction
y	Vertical image coordinate

NOMENCLATURE
(Continued)

t	Time
z	Depth-of-field of camera optics
λ	Wavelength of laser light
ξ	Diffraction-limited resolution
ξ_T	Transverse resolution of cinephotographic system
ξ_d	Depth resolution
ω	Oscillation frequency
ν	Damping rate for oscillations
ϕ	Angle between two viewing perspectives

ACKNOWLEDGMENTS

The author wishes to acknowledge the help of J. Michael Aulds in developing the electronic circuits. The concept for this experiment is due to Dr. Robert L. Glick. Dr. R. Richard Miller was very helpful in analyzing the movies and providing moral support. The author also wishes to acknowledge the help of Richard Tocci in making transparencies and stills, and of Paul F. Luehrmann, Janet L. Laird, and James J. Heinrichs in making the movies. The assistance of Andrew Piekutowski, James Higgens, Timothy Klopenstein, and Fred Pestian was critical in implementing the mechanical portion of this system. Alan Buswell provided software support. Dr. Ival Salyer suggested the use of the phenolic resin and gave much helpful advice during the course of the inhibitor experiments. Dr. Lee Cross and Ed Strader were active in the initial phase of the program. Many thanks to Ellen Bordewisch and Maria Carroll for their outstanding effort in typing the many documents pertaining to this program.

SECTION I

INTRODUCTION

1.1 AIR FORCE NEEDS

Both motor design and propellant design are abetted by detailed in-situ information on the deflagration behavior of propellant surfaces. Present understanding of the details of propellant combustion is sparse and would benefit from more detailed qualitative information, as well as quantitative information.^{1,2} More must be learned about localized, transient burning rates, their dependence on grain and binder composition and grain size distribution, and the coupling of regression rates of the various constituents in the grain. Solid propellants have a granular, heterogeneous composition.³ Consequently, local variations in their transient burning rates are expected. In fact, a spiked behavior in the local burning rate is known to occur in many propellants. If local transients couple to the acoustic field in the combustion chamber, the burning rate may oscillate, driving instabilities in the chamber.⁴⁻¹⁰ Detailed information on transient regression rates is poor. The provision of such data would be of great benefit both in propellant formulation and in motor design. The length scales of the heterogeneities range from 2 to 10^3 μm (the smallest being additives, the largest being oxidizers). Therefore, the phenomena pertaining to the combustion possess these length scales.

An experiment which provided clarity and detail for quantitative statistical analysis would be of tremendous help to the modelers. This type of information is available in high-speed movies of flows and combusting systems. Because of its high-pixel density, a photograph has great advantages for recording topographic information. Solid propellant combustion is a prime example of a system for which detailed movies can provide much-needed information. To follow both the local and transient

propellant response requires movies that simultaneously offer good spatial resolution and high framing rates. It is suspected that the combustion of individual particles is affected by their environment, possibly including other particles over regions that are quite large compared to individual particle dimensions. Moreover, the flame temperature and gas dynamics may not be properly representative of motor conditions if the cross section of a propellant test strand is too small, so it is desirable to obtain information over a wide field-of-view. Since it would also be helpful to observe the fully combusting surface for a time longer than the time it takes the largest particles in a given formulation to be completely consumed, movies should be made over extended time periods.

Much of these quantitative data could be organized in terms of correlation functions and probability density functions. This would require the automatic processing and analysis of a large number of frame sequences. It would also require high-quality films of excellent resolution and a thorough characterization of the propellants and the burn conditions.

Many propellants are worthy of detailed photographic studies, but one class of special importance lacks the high-pressure exponents typical of conventional grains. Studies by Richard Miller of Hercules Corporation show that these formulations exhibit an anomalous burning behavior as a function of grain size mix¹¹ which is not predicted by theory and is not well understood. The burning rate is extremely sensitive to the binding agent; changes in the burning rate by a factor of eight, due to the binder, have been observed. Miller found that the burning rate of the larger (400 μm) crystals follows a distinct, step-wise pattern. In many cases these grains undergo such strong changes in burning rates as to self-extinguish. Information similar to that found by Miller is needed on grains of smaller (20 μm) size.

A second important class of propellants uses aluminum as a fuel and ammonium perchlorate (AP) as an oxidizer. These formulations have a very high specific impulse but have been difficult to study, due to the opacity and luminosity of their flames. It is known that the heterogeneity of composition and grain size play an important role in their combustion, but the details of the effect of the interactions between the constitutive grains on the respective grain regression rates are not well known.

For the above reasons, the bulk of the experiments were run on wide-distribution AP propellants, with a few additional movies made on aluminized propellants. The emphasis in this program was to deliver to AFRPL a data base on the microscopic and transient combustion of propellants which can be used in models of propellant combustion.

1.2 LIMITATIONS OF CONVENTIONAL TECHNIQUES

Presently one means of obtaining the transient propellant burning rate is by the phase shift in a microwave cavity.^{12,13} The data acquired using this technique are impressive. However, it yields only an average oscillatory burning rate taken over the entire burning surface of the propellant. This technique is best suited for recording repetitive, sinusoidal oscillations and is insensitive to secular transients. Finally, it is restricted to information about the regression rate of the strand itself. It gives no information about coupling to perturbations in the gas-phase combustion zone and would not readily be extended to geometries other than end-burning strands. To date, it has only been demonstrated successfully in burns occurring inside of waveguides. The applicability of such data to environments more closely approximating practical motors is not clear. Indeed a Hilbert transform analysis of microwave data has been made, showing that these data are very inaccurate.

Additional information has been obtained from a post-mortem analysis of the surfaces of quenched propellants.^{11,14-17} Much of the detailed understanding of segregation and sintering in mixed grain formulations is based on such work. Unfortunately, it is not known to what extent the grain surface is altered during the quenching process.

Much of the present knowledge of propellant deflagration has been garnered by high-speed photography.^{14,18-20} However, cine-photography using conventional light sources is unable to resolve the burning particles hidden inside of their bright flames. Conventional cinephotography suffers from an inherent blur limitation, given by long (10 μ s) shutter time. In addition, standard window bombs do little to isolate various aspects of the chamber environment, such as the magnitude and direction of the flow relative to the propellant surface. Such movies are made with white light, with effective shutter times on the order of a microsecond. These conditions would require film motion blur of seven microns for every increment of a thousand frames per second in the film framing rate at unity magnification. In fact, these movies are usually taken with an effective shutter time equal to a given fraction of the framing rate, with a "1/100th shutter" being about state of the art. This would result in 70-micron motion blur at unity magnification.

Most conventional films are taken at framing rates of 2000 to 4000 frames per second, with the bulk of them at the lower end of that range. This would limit their ability to follow one kilohertz oscillations in detail. Conventional movies obtain their peak resolution on the order of 25 microns (15 μ m has been claimed) through magnification. Magnification has the advantage of overcoming the blur problem due to the long shutter times in these movies. It also enables the experimenter to use large-grain film which does not require extremely intense light for exposure. However, every factor-of-two increase in magnification reduces the depth-of-field by a factor of four. Consequently,

these movies must suffer not only from a reduced field-of-view due to their magnification, but also from a very limited depth-of-field. Since these movies are run without a servopositioner, this also limits the number of frames in focus within a sequence.

1.3 APPROACH

The objectives of the experiment are to develop an enhanced experimental capability for achieving high-resolution movies of propellant combustion over a wide field-of-view and an extended time period. The primary aim has been to obtain qualitative information, but demonstration of the potential of such films for providing quantitative data was also sought. The approach taken has been to assemble a photographic system comprising four key elements: a copper-vapor laser, a coherence spoiler, a photodiode array based servopositioner, and a window bomb with wide optical access.

The use of an intense pulsed 510 nm laser for illumination relaxes some of the constraints germane to white-light illumination. Consequently, it is now possible to survey an entire strand surface in detail. In this manner, meaningful statistical information can be obtained about detailed particle behavior in the flame. In particular, analyses of interactions between particles and cooperative behavior, if any, may be made.

1.4 SCOPE

The program consisted of several tasks divided into three groups. The first group involved the setup of the experiment. This included construction of a windowed combustor optimized for the experiments, checkout of a state-of-the-art copper-vapor laser, implementation of a circuit for synchronizing the laser pulses with the camera framing rate, and development of a detailed experimental plan. The second set of tasks comprised

the main focus of the proposed work--delivery of a data matrix on a sequence of selected propellants. The major goal of these experiments was to provide high-quality front-lit movies of improved resolution that enhanced our qualitative understanding of propellant deflagration. The third group of tasks consisted of attempts to extend our capability, using variants of our principal experimental technique, especially stereo cinephotography.

A customized windowed combustor was built for these experiments. The combustor was provided with a wide-angle window configuration optimized for stereo photographs of the strand surface. The combustor was TIG welded from stainless steel tubing and commercial flanges. Circuitry to synchronize the laser pulses with the camera framing rate was designed and installed. A servopositioning circuit to maintain the strand surface within the depth-of-field of the camera optics was also designed and fabricated.

The main work consisted of front-lit profile studies of localized regression rates of a series of related propellant strands and their analysis. In the beginning, a matrix suggested by Richard Miller was used. The formulations were of ammonium perchlorate (AP) grains using IPDI and DDI curatives. Ten percent of the grain mix consisted of 20- μm particles. Two-thirds of the mix consisted of 400- μm and 2- μm particles in a five-part series of respectively 38/39, 41/36, 44/33, 47/30, and 50/27 percent. The remaining 13 percent of the formulation consisted of binder. Three pressures were used: 500, 200, and 100 psi.

In addition to the matrix movies, front-lit high-speed stereo movies were also made of the burning surfaces of solid propellant strands at operating pressures up to 350 psi. Movies were made at viewing angles separated by 90 degrees to achieve a high depth resolution. These movies, which were recorded through flames across a $\frac{1}{4}$ in. field-of-view, have a resolution of 25 μm . The

stereo images were simultaneously recorded side by side on the same 16-mm frame by using X2 demagnifying optics and a mirror arrangement. The two images then passed through a single camera lens. Because of the complexity in the acquisition and reduction of stereo data, quantitative data analysis of stereo movies was attempted. This effort was undertaken solely to demonstrate feasibility and to provide qualitative information.

SECTION II

EXPERIMENTAL DISCUSSION

This section describes the experimental apparatus and procedures. Approaches to various experimental problems are also discussed, as are the specifics of those problems. The first four paragraphs cover hardware, optics, and electronics. Minor efforts to support the photography program and a description of the photography experiments are given in the remainder of the section.

2.1 HARDWARE

A versatile seven-port window bomb was constructed with provisions for ease of maintenance and plentiful optical access (Figures 1 and 2).²¹ High-resolution movies demand extensive optical access, with ruggedness against window fouling, which is a special challenge for front-lit movies, since the camera must look down on the surface. The design chosen features several large reentrant viewing ports (Figure 3), allowing for optics as fast as $f-1.3$ to $f-2$. The chamber was made large (8 in. diameter by 14 in. height) to facilitate maintenance and minimize light attenuation from smoke. Problems with smoke were further reduced by the use of a high throughput purge that was primarily directed over the windows. The three ports on the back side of the bomb were provided for stereo photography. This window bomb has all the optical access needed for the experiment.

The pressure chamber was welded and stress relieved. Welding distorted the ports by as much as 45 thousandths, more than had been anticipated. The seals on the windows only allow for variations in dimension of ± 0.005 inches. This necessitated re-machining the ports and their sleeves. Chipping of the two inch-diameter BK-7 windows used in initial experiments was noticed.

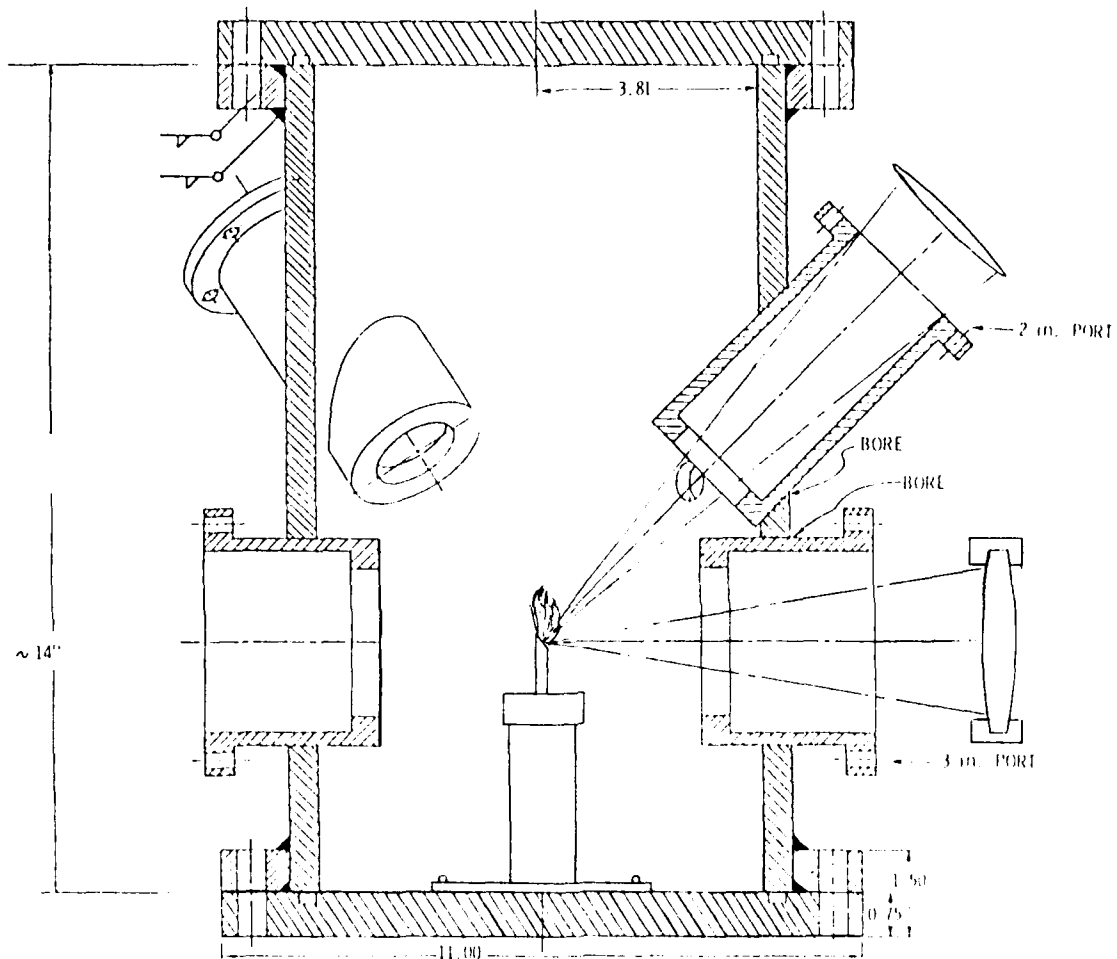


Figure 1. Cross Section of Window Bomb. The laser illumination is from the horizontal direction. The camera views the strands from a 45° angle, directly through the flame across the surface.

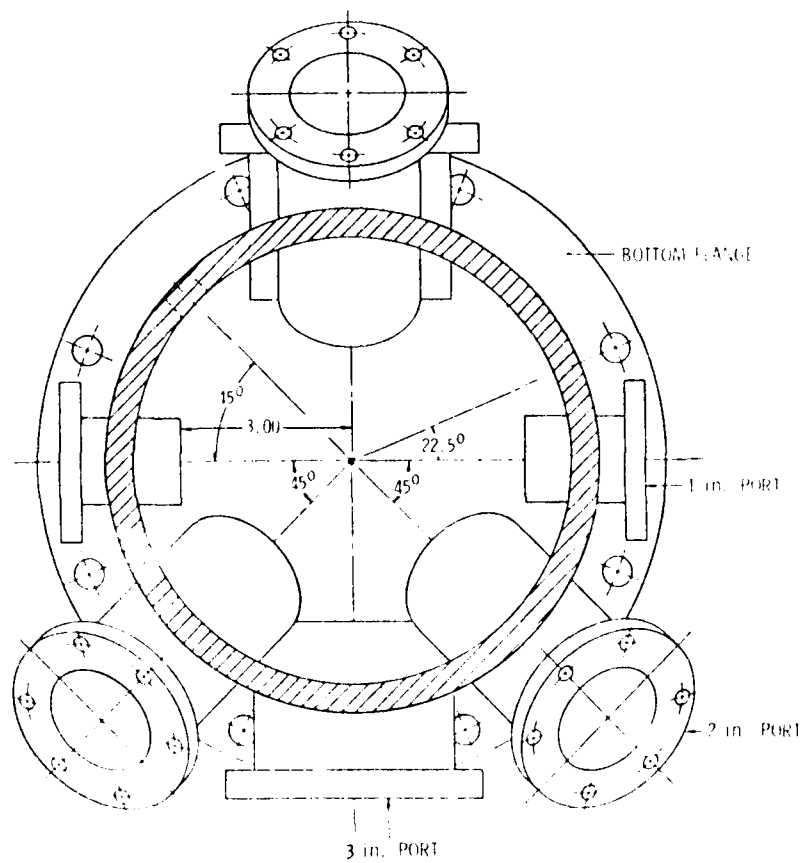


Figure 2. Top View of Window Bomb. Reentrant ports allow plentiful optical access while minimizing the size of the bomb.

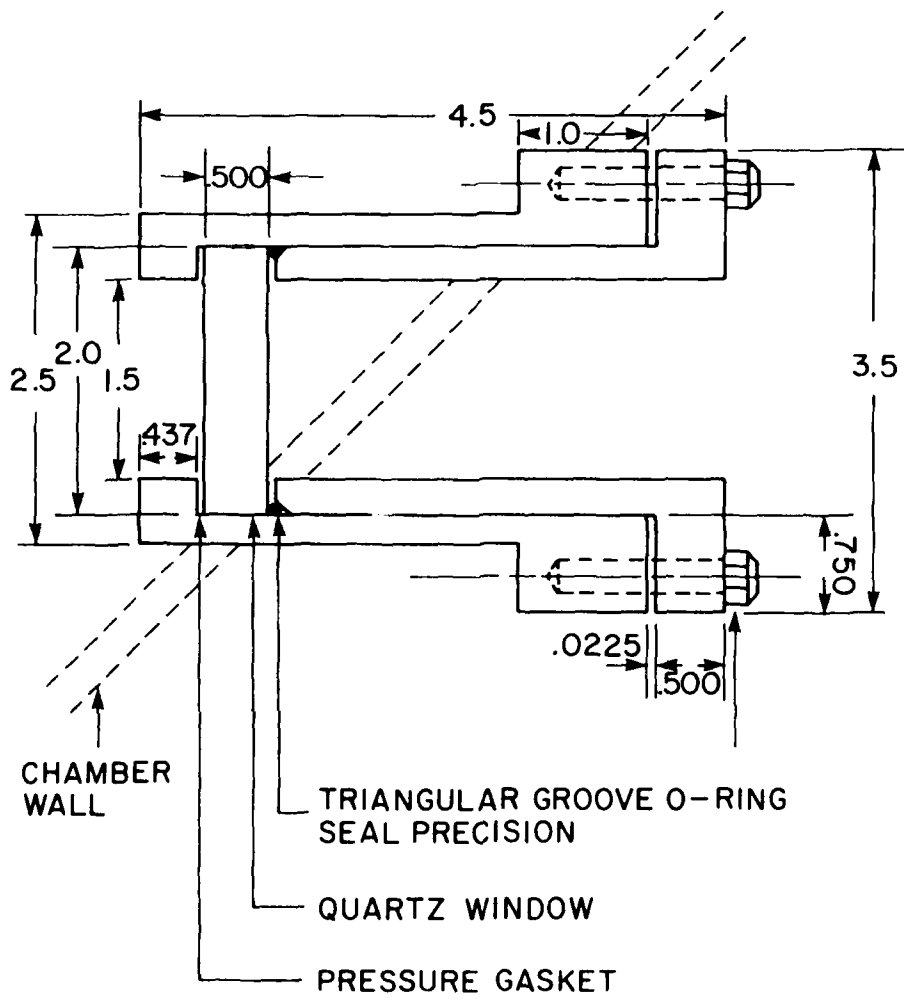


Figure 3. Reentrant Window Port. This design maximizes optical access.

This chipping was probably due to radial stresses, and it was in part related to the tight fit between the windows and the port sleeves. The chipped windows were replaced with quartz windows which were precision ground to match the port dimensions.

The interior of the chamber was painted with an epoxy coating to retard corrosion from the hydrochloric acid produced by strand combustion. An enclosure, built around the window bomb, consisted of two-inch-thick wood laminations; it was designed to yield, rather than rupture, should the pressure chamber fail. A secondary safety barricade was erected between the pressure chamber and the control area. The safety precautions included the purchase of ear and face protectors, miscellaneous safety modifications of the electronics and power supplies, and safety baffles to enclose the laser beam.

The window bomb design has allowed turnaround times between filmings as short as 30 minutes. In addition to reentrant windows with seals that allow for flexibility in viewing placement, other innovations in the chamber design include pressurization inlets at the chamber windows rather than at the strand to minimize window fouling and a mechanical strand mount to minimize turnaround time. A strand guide that minimizes frictional drag on the propellant was also developed; this allows the servosystem to make rapid corrections of the strand positions.

Due to the narrow (200-600 μm) depth-of-field restriction imposed by diffraction limitations and the high-resolution requirements, a rigid frame was built to hold the high-speed camera, window bomb, and servocircuit at fixed distances from each other despite their separation by one-meter distances. A thick metal table top and Unistrut frame supported the fuel combustion chamber on four adjustable legs. The thick metal plate served to focus and unitize the function of the other elements which completed the experimental setup. Two of the

three legs of the camera tripod, the fuel-feed mechanism, and the servo-optics were also attached to this plate. The front pair of legs supporting the camera maintained a fixed film-to-target distance.

The third leg of the camera tripod, the fuel-feed mechanism drive motor, and several other items were also attached to the Unistrut frame using smaller metal plates. Thick rubber pads used in the construction of the camera tripod feet greatly reduced transmission of vibrations between the camera and fuel chamber/fuel feed mechanism and other system elements. The camera/microscope assembly was rigidly attached to the tripod once proper alignment of the camera had been ensured. The height of the frame was reduced horizontally by mounting the motorized translation stage for the servosystem which drives the propellant strands. Vertical motion of the strands was obtained by means of a triangular cam. This feature allowed lowering the overall height of the frame about 15 inches, improving stability. It also increased the stability of the mounting for the translation stage. In addition, a lower overall height facilitated operation of the system and added to safety.

The propellant was ignited using a wire filament and a high current pulse. A portion of the pressurizing gas that flowed along the sides of the strand tended to break the ignition wires, so wires were made that were doubly wound except in their centers. The ignition wires were fastened to heavy copper leads that clipped in place and could easily be removed from the chamber.

The sides of propellant were coated with an inhibitor to prevent flashing. The performance of traditional inhibitors, such as silicone grease, was not satisfactory for this work, due to smoke formation and incomplete inhibition. Testing of alternate inhibitors has shown that a partially reacted phenol-formaldehyde polymer works very well as an inhibitor on

propellent strands, provided that it is properly prepared with an appropriate solvent.²²

2.2 OPTICAL SYSTEM

Due to the high resolution sought and the physical limitations of the experiment, the work performed pushed physical limits. These limits and the optical design chosen are discussed in the following paragraph.

2.2.1 Physical Limits

In the geometry used, the camera looked down on the strand surface through the flame and the laser illumination was directed from the horizontal direction. The strands were cut at a 45° angle to match the 45° viewing angle of the camera (Figure 1).

The standard method of dealing with film motion blur in conventionally illuminated high-speed photography is to use magnifying camera optics.²³ The blur as a percentage of the frame size remains the same, but the corresponding absolute size of the blur is reduced. For example, a magnification of four in a 16 mm film with a 1/100th shutter should give less than 20 μm of film blur. Additional advantages accrue from this approach, since the lenses in standard cameras, projectors, and enlargers do not work well at dimensions below about 25-40 μm, and the demands on film grain size and sensitivity are not severe using magnification. However, for a fixed frame size, magnification severely limits the field-of-view (to less than 2 mm in a 16-mm film using a magnification of four), a result contrary to our prime objective. Furthermore, the depth-of-field (the distance through which the object remains in focus to the camera) falls off inversely as the square of the magnification. High-resolution imaging requires fast optics. The f-number, $f\#$, of a

lens is given by the ratio of its focal length, f , to its diameter D :

$$f\# = f/D \quad . \quad (1)$$

The diffraction limited resolution, ξ , of an imaging system, is given by²⁴

$$\xi = 1.2 f\# \lambda \quad , \quad (2)$$

where λ is the wavelength of the light used. At visible wavelengths with an effective $f\#$ of 8 the diffraction-limited resolution is about $8 \mu\text{m}$. The depth-of-field, z , is related to the resolution of the camera optics, b , by²⁵

$$z = f\# b \quad . \quad (3)$$

If b is at the diffraction limit, ξ , we have

$$z = 1.2 (f\#)^2 \lambda \quad . \quad (4)$$

For a resolution of $20 \mu\text{m}$ and an $f\#$ of 8, z is on the order of $160 \mu\text{m}$. This can be significantly less than the dimensions of the larger particles, let alone the large-scale variations in surface topography due to the vagaries of heterogeneous combustion. The depth-of-field limitation becomes even more stringent with magnification. For a given magnification, M , Equation (4) is modified to

$$z = 1.2 (f\#/M)^2 \lambda \quad . \quad (5)$$

Since the depth-of-field problem is aggravated by flame turbulence at pressure, due to changes in the optical path length, magnification virtually precludes movies of extended length on fully combusting surfaces of appreciable area. Of course, for a fixed film frame size, the field-of-view also

decreases as $1/M^2$.²⁴ For the above reasons it is often preferable to demagnify rather than magnify the film images. This approach places heavy demands on the quality of the camera lens and the resolution of the film used, as well as on any lenses used in the reproduction or projection of films. Although it has been possible to obtain useful quantitative data using demagnification, the resulting films lack visual clarity. The production of movies with easily discernible features requires high-contrast images, which are especially difficult to obtain from a low-contrast subject. The problem of preserving image contrast leads to the concept of the Modulation Transfer Function.

All lenses, as well as photographic film, act as low-pass spatial filters; i. e., the signal from small features is severely attenuated relative to the signal from large-scale objects. The surfaces of the propellant strands on which our experiments are made have little contrast. As such, the movies of their deflagration are especially affected by the falloff in contrast of any optical system with the inverse of the spatial dimension of interest. The inverse of the spatial dimension is referred to as the spatial frequency, k . The reduction in image contrast due to the low-pass behavior of the lens and film is described by the Modulation Transfer Function (MTF).²⁵ Since any object, such as a standard bar chart, can be represented by a superposition of cosine fringes, we consider a cosine fringe pattern of frequency k represented by $I(x) = 1 + m \cos(2\pi kx)$.

The modulation is defined by

$$MTF(k) = \frac{I_{\max} - I_{\min}}{I_{\max} + I_{\min}} = \frac{(1 + m) - (1 - m)}{(1 + m) + (1 - m)} = m. \quad (6)$$

The modulation m is equivalent to the fringe contrast. When the fringes are imaged or recorded, their modulation is attenuated by

an amount which depends on the fringe frequency. This attenuation factor is the MTF of the lens or film under consideration (Figure 4). The absolute upper frequency limit on the MTF for a lens is set by the lens aperture-film combination. The cutoff frequency of the camera system, k_c , is given by

$$k_c = \frac{1}{2\lambda f^\#} \quad (7)$$

A real lens will have an MTF that decreases out to this limit. Obviously, if the contrast of the subject is less than one to begin with, a small value of the MTF will drive the resultant contrast of the image below the detection limit, well before the frequency cutoff of the MTF is reached. Typically a much lower spatial frequency, k_1 , will apply, since the quality of the image will degrade steadily as k_1 increases, especially with low contrast object fields. Often k_1 is taken to be about $k_c/4$. The required relation for ξ is:²⁶

$$\xi = 1/Mk_1 \quad (8)$$

Therefore it is desirable to maximize k_1 . Unfortunately, z obeys the relation²⁶

$$z = \frac{1}{(Mk_1)^2} - \frac{1}{\lambda} \quad (9)$$

for light of wavelength λ . Therefore, high-resolution movies with a practical depth-of-field must be made at low magnification. Note that ξ and z are coupled, with

$$z = \xi^2/\lambda \quad (10)$$

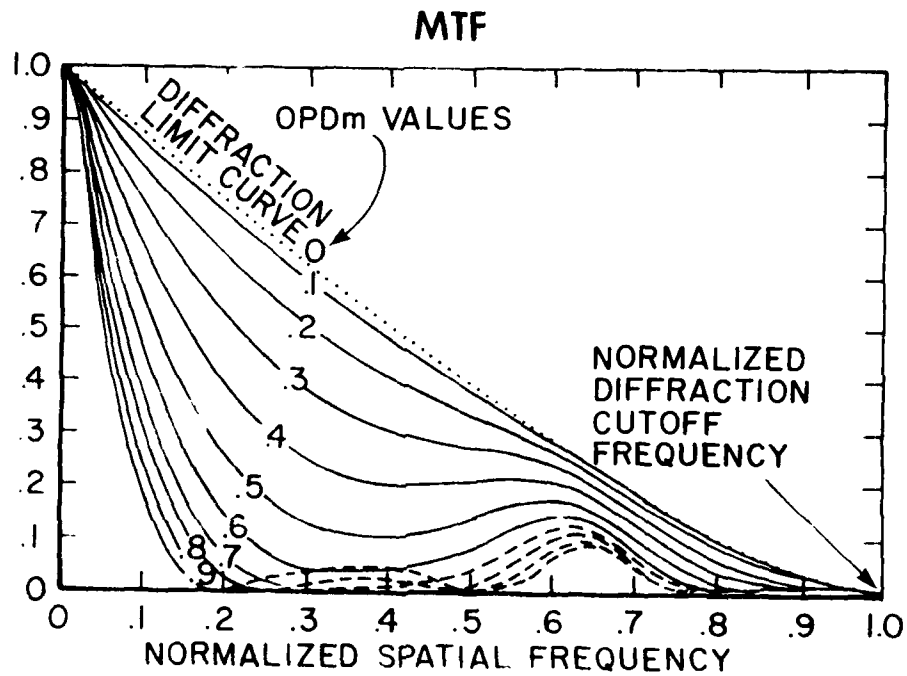


Figure 4. Modulation Transfer Function of Typical Single-Element Lens. Note that the monochromatic curve is vastly superior to the polychromatic curve. Reprinted with permission of Melles Griot Corporation, Ref. 2.

This places severe limits on the system as ξ approaches λ . To complicate matters, the overall MTF of a system is the product of the component MTFs, as very high quality components must be used at every step. This includes the MTF of the film (Figure 5). Please note that MTFs are much worse for white light than for monochromatic light (Figure 6).

As a rule of thumb, the highest usable frequency passed by an optical system is about one fourth of the usable MTF cutoff. The detection limit of the system is the inverse of the usable MTF cutoff. To be resolved, an object should be twice as large as the detection limit, and to be well resolved it should be four times as large as the detection limit. For example, to image a 20-micron object, at least a 10-micron resolution is desired, which corresponds to 100 line pairs/mm. Ideally, the MTF of the imaging lens should even extend out to 400 line pairs/mm. At $\lambda = 0.51$ microns (the copper-vapor wavelength) the lens should ideally operate at an $f\# = 2.5$. A trade-off must often be made between detail in a film and visual quality. Low-contrast features are most severely affected by the fall-off of a lens/film system MTF with decreasing feature size, so that small-scale, low-contrast details tend to fuzz out. Large-grain film and a high-contrast developer result in a film with good visual clarity, while a fine-grain film and a soft developer give a more faithful representation of the object field. Similar considerations apply to reproductions, whether by motion picture projectors or enlargements of individual frames. The fine detail obtained in a soft picture leads to a blurred result in reproductions using standard commercial equipment.

The best MTFs can be obtained for an optical system which is very close to the subject, as in a microscope. Unfortunately, very small object distances are not practical in combustion photography. The need to protect the camera lens, the need to obtain a reasonable depth-of-field, and constraints imposed by the design of a camera at unity magnification require a minimum

FILM MODULATION TRANSFER CURVE

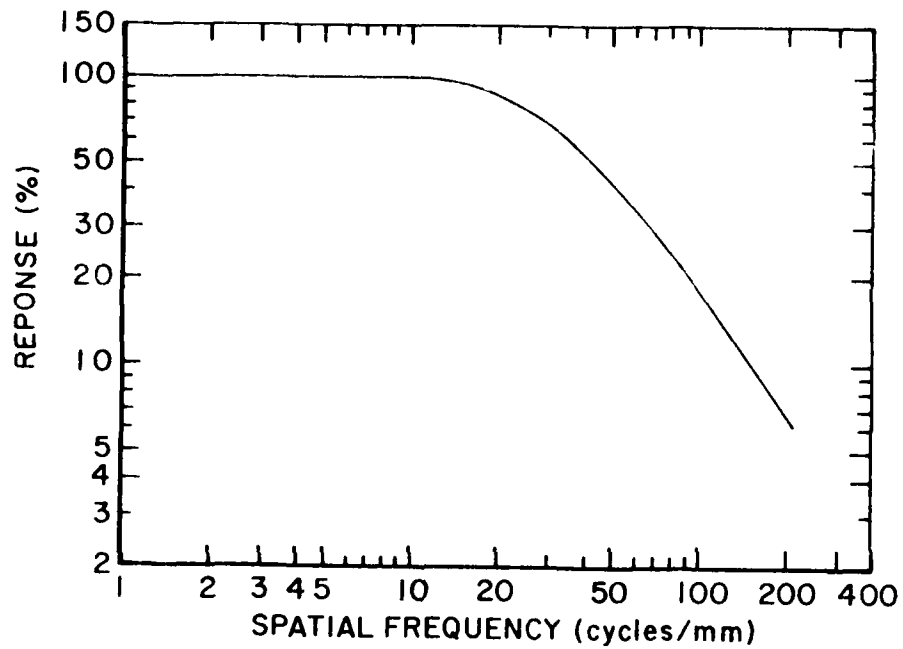


Figure 5. Modulation Transfer Function (MTF)
of Film. This low-pass curve is
multiplied by the MTF of the camera
lens, impairing the contrast of the
features. Adapted from Eastman Kodak.

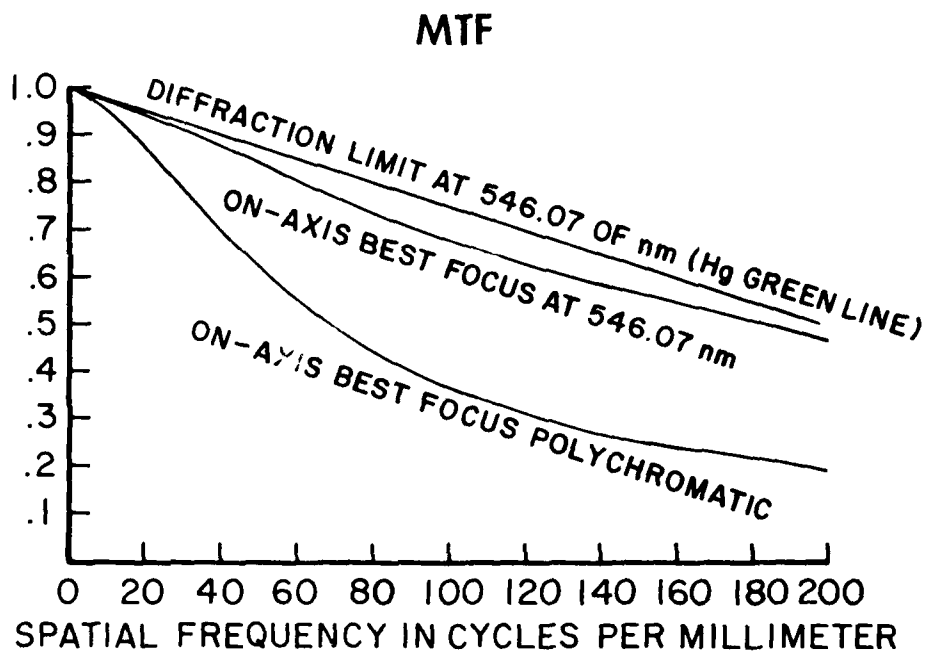


Figure 6. Modulation Transfer Function of White Light vs. Monochromatic Light. Due to chromatic aberrations, superior contrast can be preserved with monochromatic light. Adapted from Melles Griot, Ref. 2.

object distance on the order of 100 mm. Provisions for such a minimum distance were made in the design of the window bomb. Using standard high-quality optical glass, this constraint and the need for a manageable depth-of-field lead to a maximum lens f-number of about 6-7. At unity magnification this would give a cutoff spatial frequency of about 150 line pairs/mm. Smaller lens f-numbers cannot be used since they would seriously impair the depth-of-field.

The MTF falls off rapidly as the field-of-view is increased (see Figure 7). For a 1/4-inch radius and a 5-inch object distance the paraxial angle will be as much as 1.5°. This poses no severe difficulties for monochromatic light. However, it seems that an enlarger lens and a projector lens should be designed for large image distances. A curved screen may be helpful for movies.

2.2.2 Optics

All of the movies in the experiment were made at a magnification M of 1 or 0.5. The depth-of-field was estimated as less than 200 μm at unity magnification and about 600 μm using a demagnification factor of two. A Nikon 50-mm Nikkor f/4 micro lens was used in the experiments. This lens was rated at a resolution of 100 line pairs/mm and was tested at a resolution of 6 μm on high-contrast images. Unfortunately, most of the propellants studied had low-contrast surfaces in the absence of any contribution from flame emission. Consequently, the MTF of the lens-film combination limited the best resolution to about 20 μm . Typically, the smallest identifiable features in these films measured about 25 μm . The Nikkor lens was designed for operation in a demagnifying configuration, with a demagnifying ratio of 2:1. Most of the movies were filmed in this demagnifying configuration to extend the depth-of-field. Films of strand ignition on stationary propellants were made at unity magnification using an additional lens element. This resulted in a further degradation of the MTF of the camera lens.

MTF

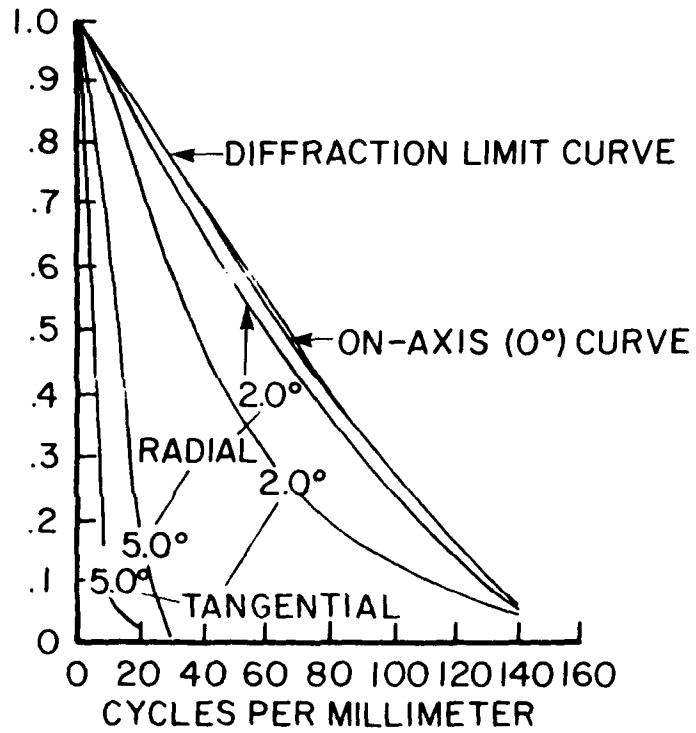


Figure 7. Modulation Transfer Function vs. Field of View. Performance falls for non-paraxial rays. Reprinted with permission of Melles Griot, Ref. 2.

The sighting scope on the camera was inadequate for proper focusing on microscopic targets. A new sighting scope was designed for the camera, since the existing sight did not possess sufficient resolution to achieve satisfactory alignment. This scope used a microscope objective mounted behind the camera. The location of the focusing scope relative to the camera was maintained by mounting to a heavy ($\frac{1}{2}$ -in. thick) aluminum plate.

Laser speckle is a common problem in high-resolution photography. Film tests showed that the copper-vapor laser had sufficient coherence to induce laser speckle. This problem was met by inserting an ellipsoidal coherence spoiler in the input optics (Figure 8). The 510 nm copper-vapor laser light was focused on a stainless-steel ball coated with magnesium oxide powder. The light scattered by the rough surface of this ball was collected by an ellipsoidal mirror and focused on a target. The spoiler has been tested using both a 632.8 nm He-Ne laser and the copper-vapor laser. The spoiler succeeded in eliminating almost all of the speckle from the He-Ne laser--a severe test.

2.3 SERVOPOSITIONING CIRCUIT

A servopositioner was developed to locate the position of the surface of a strand of rocket propellant as it burned in an irregular fashion.²⁷ A concomitant of high resolution in a photograph is a very shallow depth-of-field.²⁸ In this case the depth-of-field was sometimes as small as 200 microns. Since the propellant burned at a rate of one to four centimeters per second, only about two-hundredths of a second were available during the course of a normal burn in which the propellant would be within the proper depth-of-field. However, because it was desired to take movies over a period of several tenths of a second, it was necessary to continue to push the strand forward to maintain the surface within the depth-of-field. This task was not simple, because propellants burn in a highly irregular fashion and there are local irregularities on the heterogeneous

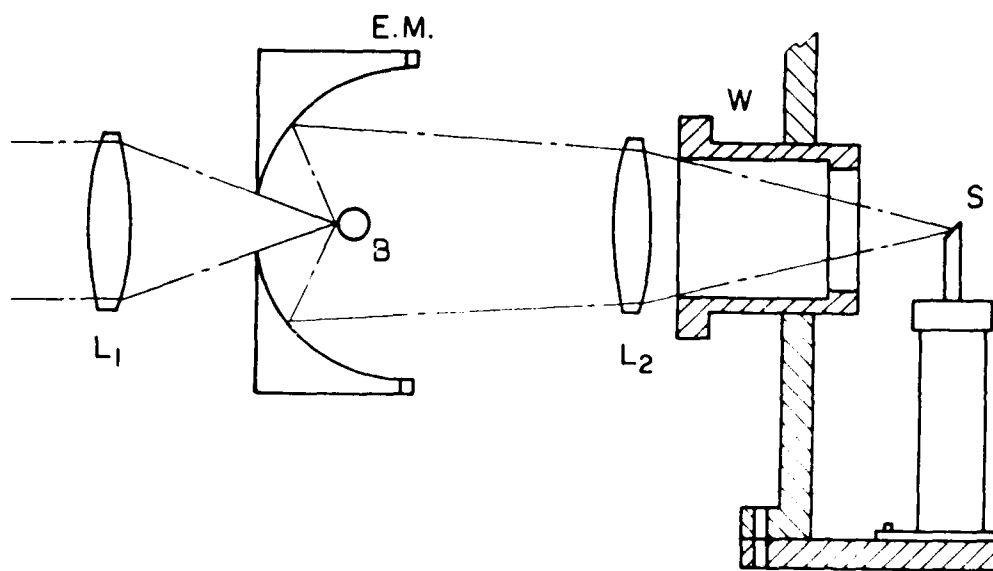


Figure 9. Coherence Spoiler. The large diameter angle given by the ellipsoidal mirror and the powdered surface of the ball at one of the mirror's foci successfully eliminate laser speckle.

surface itself which can be as much as 400 microns in size. Hence, it was necessary to design a circuit which could compensate for the motion of the burning strand and the idiosyncracies of the mechanical drive, and continue to locate and hold smoothly the position of the surface to very tight tolerances.

The problem is made more difficult because intense smoke is generated by the burning of the strand. This smoke interferes with the intensity of a laser light beam used to sense the position of the burning strand, and furthermore the smoke will foul windows used in the pressurized chamber. These problems make the use of a single-detection element unsuitable, as that detection element would then become sensitive to the amount of smoke and the amount of fouling of the windows, rather than to the true position of the strand. For this reason, as a sensing element an array of photo-diodes was chosen, each of which had a given threshold level above which the diode would fire and would produce a unit signal. The total signal determining the position of the strand then was given not by the total light level falling on the array, but by the number of diodes in the array which were either on or off.

Previous opto-mechanical servocontrol units used only one or two photo-diodes as detection elements.²⁹ As such, they were not highly rugged to smoke or window fouling, and had fundamental limitations on the tightness with which they could control the location of the target. They had no special optics for concentrating the range of the target or eliminating flame luminescence. They were limited in their ability to follow an irregularly moving object. By contrast, the circuit used here was insensitive to flame illumination, smoke, and turbulence, was highly agile, and afforded excellent position control.

2.3.1 Opto Mechanical Subsystems

Our system had three parts: a mechanical drive (Figure 9), an optical part (Figure 10), and an electronic circuit. The fuel

MECHANICAL DRIVE MECHANISM

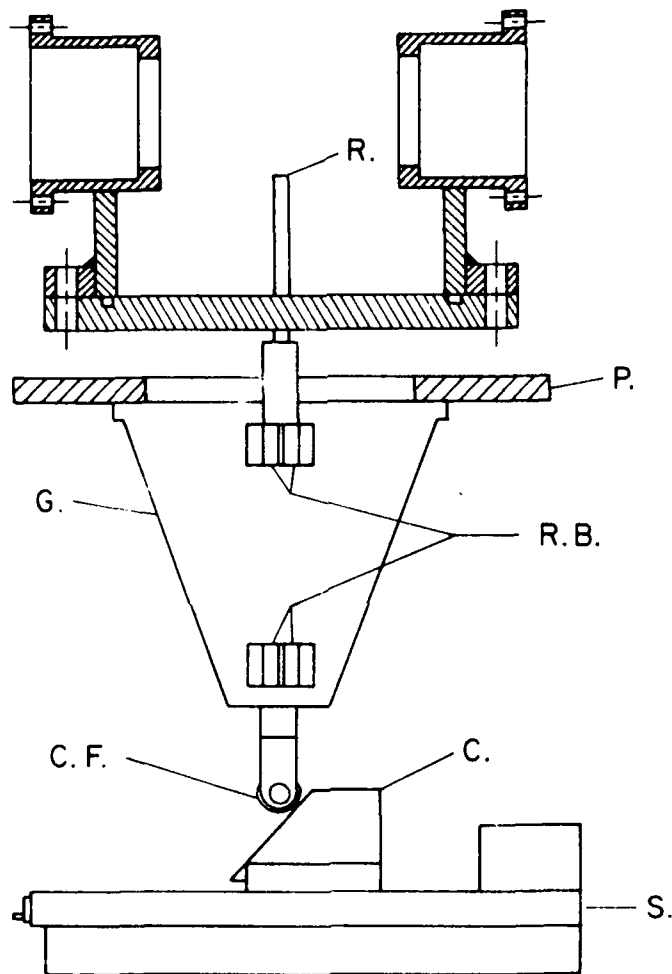


Figure 9. Mechanical Drive for Positional Controller. The horizontal mounting on the slide saved space, preserved the stability of the overall system, and gave flexibility in determining the ratio between the strand travel and the slide travel. R designates the push rod, P the chamber mounting plate, G the guide for the push rod, C the cam, S the slide, RB the roller bearings, and CF the cam follower.

SERVO OPTICS

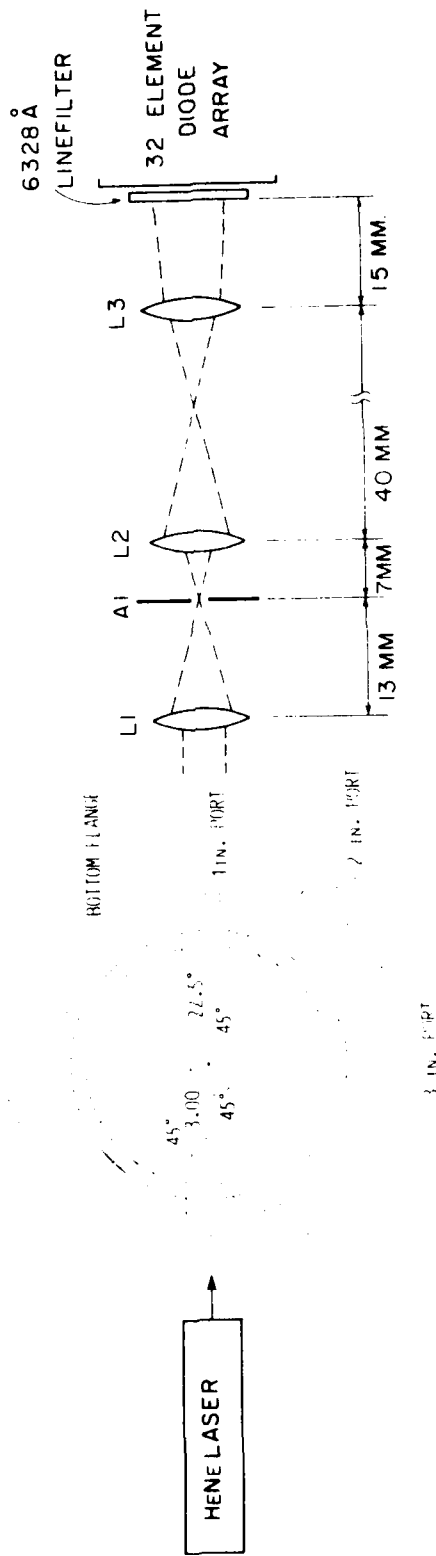


Figure 10. Servooptics. The propellant surface location is sensed by the degree of attenuation at the laser beam. Lenses are designated by L. The aperture, A1, restricts the signal to the vicinity of the strand surface. The line filter passes the 632.8 nm laser signal while blocking noise from flame emission.

feed mechanism consisted of a nonrotating, ball-bearing-guided push-rod attached to the underside of the chamber mounting plate and a motor driven triangular cam attached to a Unistrut frame. A maximum push-rod stroke of two inches was possible. The push-rod rate of advance, as a function of motor speed, could be varied by changing the wedge-shaped cam shown below the roller bearing at the end of the push-rod. The ball-bearing guide ensured that the push-rod will move smoothly without flexing under the horizontal load of the translation stage. The stage mounting block was adjusted and a mount for the entire motorized assembly was built to ensure a smooth drive of the strand shaft. The limiters were removed from the control box, which increased the rate at which the servomotor could respond.

The diode array detector for the proportional drive servo-control was a circuit (Figure .1) which provided information on the position and velocity of the irregularly moving surface. Ablating propellant surfaces have erratic trajectories and need to have their position compensated if a smooth trajectory is desired. In many cases this is relatively simple to achieve, but this circuit dealt with a case in which there was a great deal of noise on the information channel which provided the instantaneous location of the surface and in which the trajectory was in fact highly erratic. In these cases, if tight control is desired, it is necessary, due to an inherent lag in any mechanical control of the surface, to anticipate the motion or future position of the surface to be controlled. This required the ability to derive the surface velocity. There were not enough elements in the array to make an accurate determination of the acceleration. This circuit totaled the signal from an array of sensing elements, each of which was either in an "on" or "off" mode, depending on a threshold level set for each and the level of the signal input to each sensing element. Use of an array of on or off sensing elements is especially helpful in cases where the signal channel is subjected to noise. Since an optical signal was employed and the optical path was subject to interference

from smoke or dirt on windows, this system was especially rugged. The circuit was especially useful in conjunction with a proportional control on the mechanical part of the servosystem. This helped to avoid overshoots and erratic motion. In brief, this circuit involved a multielement, nonlinear servocontrol, which incorporated all of the peculiarities of the entire servosystem in its calculations.

Each element or pixel in the array corresponded to a surface displacement of 50 μm ; consequently the capture range for the system was about 1.6 mm. The circuit made use of two input signals: the location of the surface, and the time integral of the difference between this location and a reference position (error signal). The servocircuit sensed the position of the strand surface and provided a reference voltage to the controller on the slide motor. It had a proportional drive based on individual on/off signals from 31 elements in a photodiode array. These features provided a smooth control and resistance to fouling of the windows.

2.3.2 Control Circuitry

The servoposition controller was made up of three printed circuit boards (Figures 12-14). The first was the detector and analog conditioning board (Figure 12). The second board (Figure 13) was the digital processing board, and the final board (Figure 14) was the analog controller. The output from the analog controller board drove the slide controller. The slide controller moved the propellant strand up as the propellant burned down to maintain the burning surface at the same position relative to the camera lens. The detector was a Hamamatsu S994-19 32 element array. Since 0 V is a valid signal, the number of possible data outputs is equal to $N + 1$, where N is the number of photodiode elements used. Since the computer could only accept 32 possible input voltages, only 31 of the 32 elements in the photodiode array

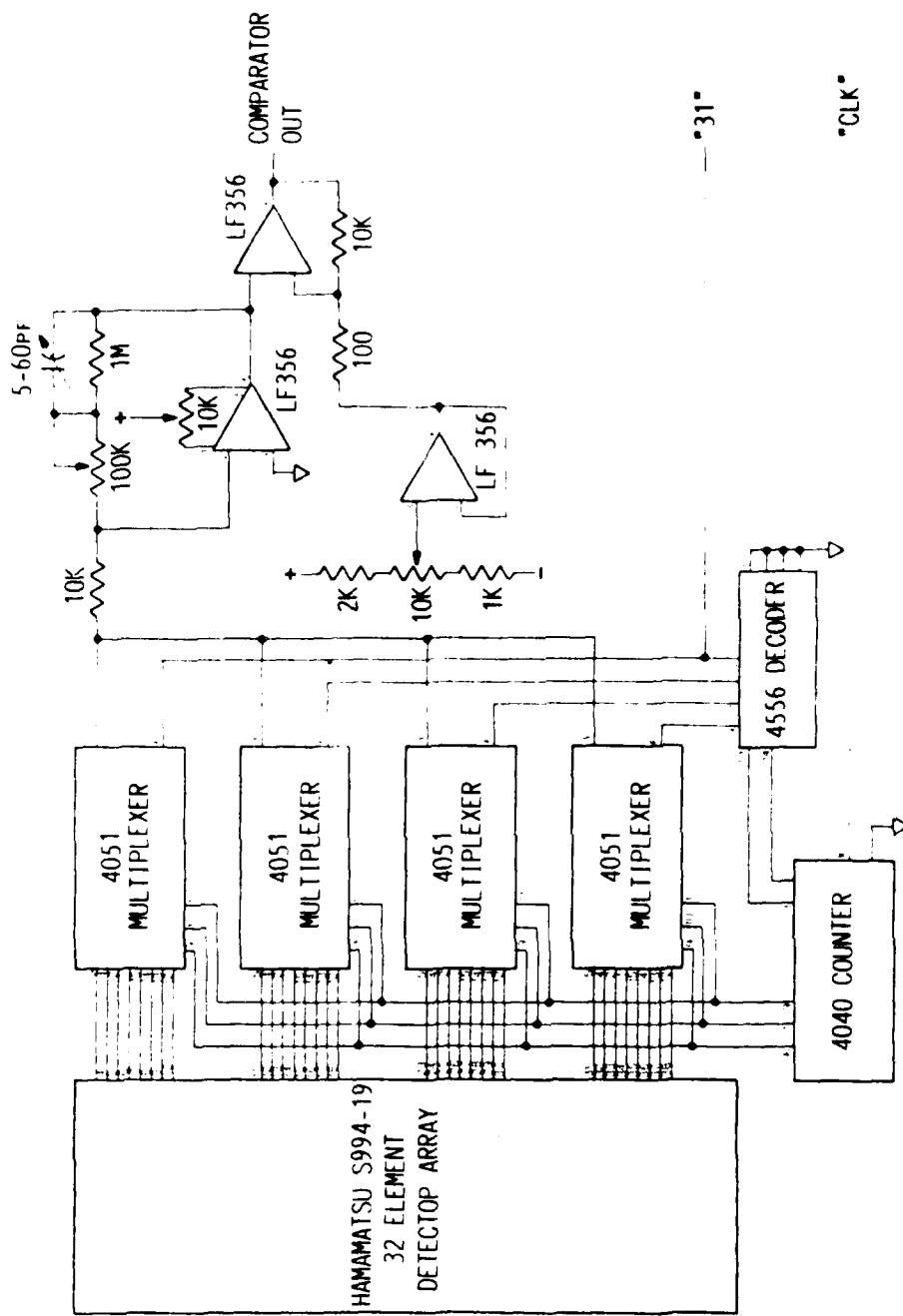


Figure 12. Detector and Analog Conditioning Circuit. Each detector element is sequentially switched to an amplifier and level comparator.

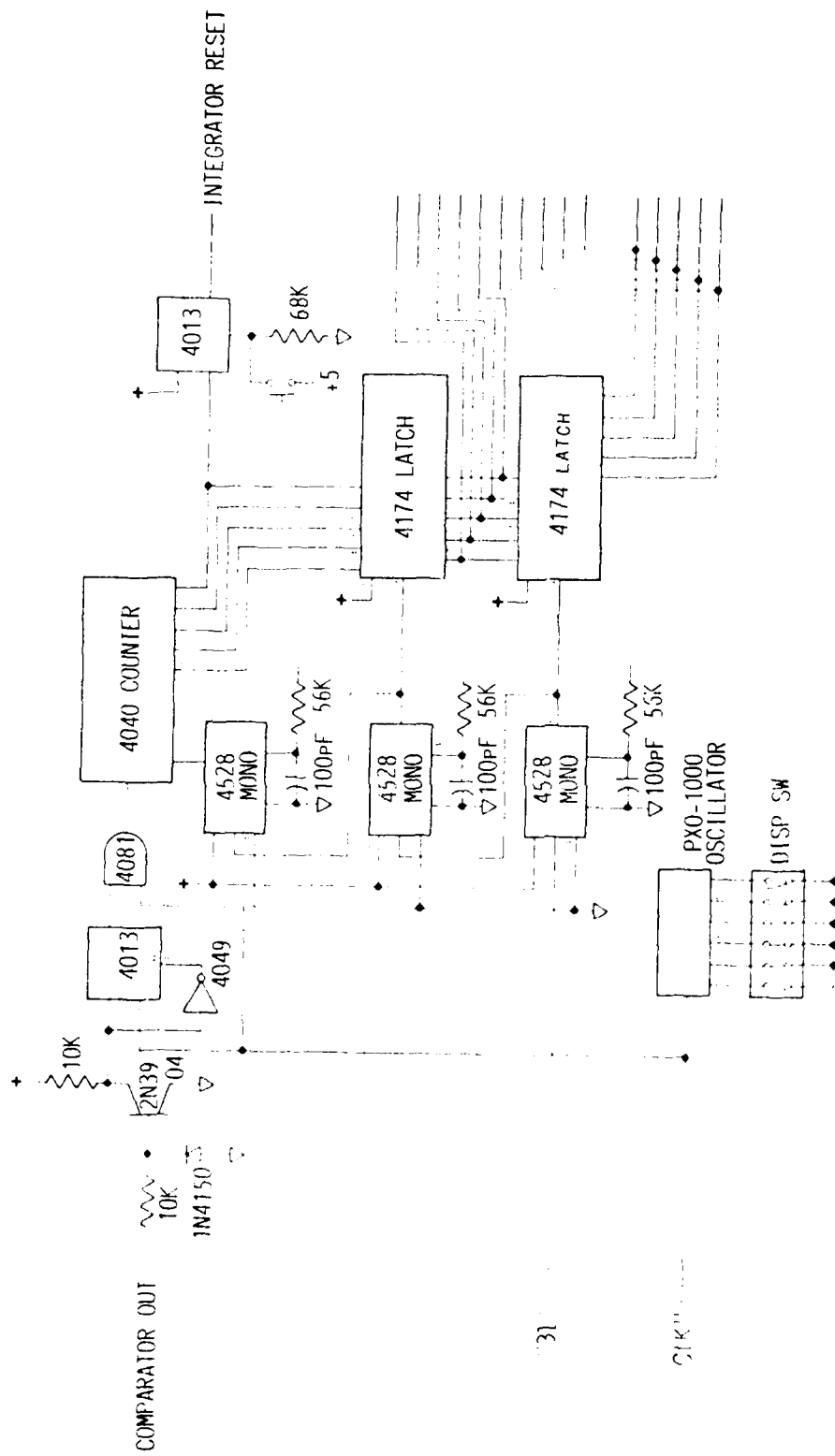


Figure 11. Digital Processing Circuit. The number of elements above threshold is counted and stored.

INTEGRATOR RESET

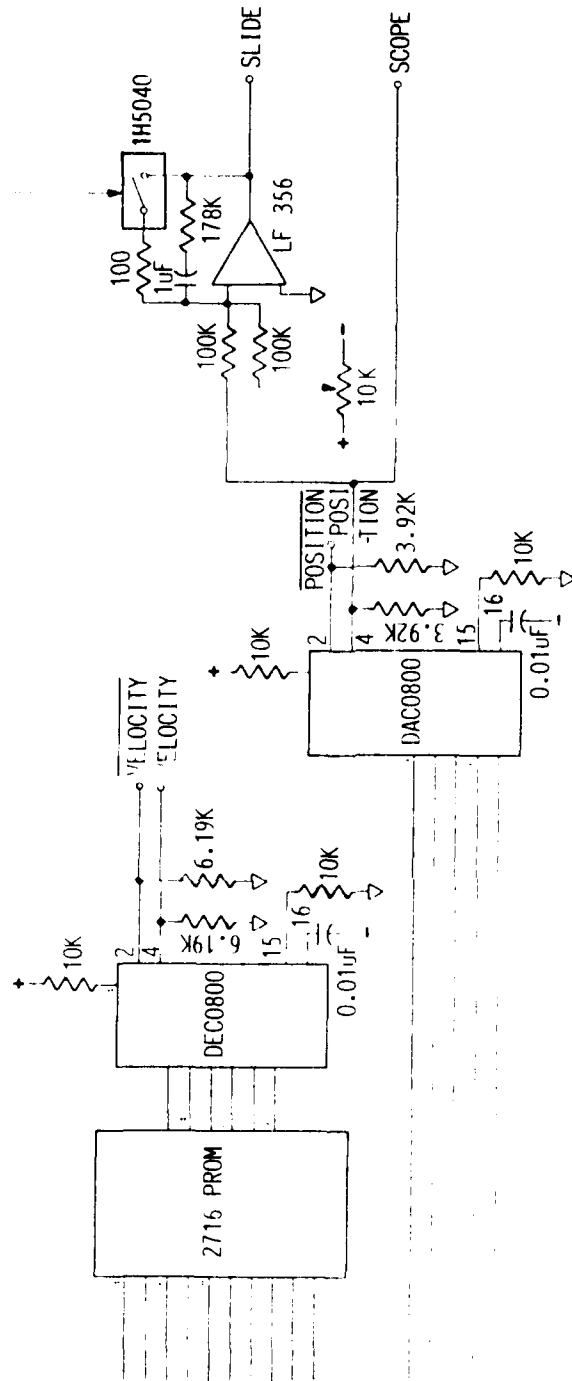


Figure 14. Analog Control Circuit. Each detector element is sequentially switched to an amplifier and level comparator. A PKOM takes the difference between two latch outputs to form a signal voltage.

were actually used. Each detector element generated a positive voltage when exposed to light. The analog processor board sequentially switched each detector element to an amplifier and level comparator. If the light level on a detector element was above a preset threshold, the output was high; otherwise it was low.

The second board took this signal and counted the number of elements above the threshold. When 31 elements had been compared with the threshold, the value of the counter was stored in the first latch, after the previous value of the first latch was saved in the second latch.

The third board took the outputs from the latches and used a programmable read-only memory (PROM) to take the difference between them. The difference was proportional to the velocity error between the slide and the burning propellant. The output of the first latch was proportional to the positional error of the propellant.

In this circuit implementation, only the position error was used as an input to the analog controller. The controller consisted of an integrator, with a resistor in series with the feedback capacitor to provide damping. The setpoint and signal were connected to the inputs. The difference between the input and setpoint was integrated and the resultant integrated difference signal was used as the proportional input used to drive the slide controller. A flip-flop was held in the reset mode when the manual reset switch was depressed. This flip-flop controlled an analog switch which held the integrator in a reset mode. When the detector changed from more than half dark to less than half dark, the flip-flop toggled, and the circuit started in the controlling mode.

The main nonlinearity in the system was due to the difference in velocity between the forward and reverse directions, because of the unidirectional drive on the slide. The servocontroller

regulated the slide velocity in only one direction (the difference between the burn velocity and the slide velocity), whereas the velocity in the reverse direction was determined solely by the burn velocity of the fuel. These differences placed constraints on the servocontroller design. Another source of nonlinearity was the detector. The spacing of the detector elements might have been nonuniform, resulting in a nonlinear positional response. The sensitivity of the individual photodetectors was also subject to variations, as was the energy profile of the laser, resulting in a shift of the detector threshold that could produce a positional nonlinearity.

To start a test, the fuel was positioned so that more than half of the detector elements were dark, the reset switch was depressed, and the slide controller was turned on. When the fuel burned down exposing more than half of the elements, the flip-flop was toggled and the integrator was allowed to operate.

An early version of this circuit used only 8 elements in the photodiode array (Figure 15). The 8-element diode array performed unsatisfactorily because the capture range of the array was too small and the attempted precision was too great. Increasing the number of elements used in the detector circuit from 8 to 31, and increasing the distance surveyed by each element from 25 μm (0.001 in.) to 50 μm (0.002 in.) increased our capture range from 100 μm (0.008 in.) to 1.6 mm (0.064 in.). Tests showed control to within two pixels, or 100 μm . Attenuation of the 632.8 nm He-Ne laser beam due to smoke corresponded to a signal drop of less than 50 mV. The voltage to each diode in the array was about 80 mV, so beam attenuation due to smoke corresponded to a position error of less than 50 μm . Initial immunity to fogged windows was not as great as we had hoped, possibly due to marginal (2mw) laser power. Fouling of the windows was subsequently minimized by directing part of the pressurizing gas directly over the window (the bomb uses a continuous flow of pressurizing gas).²²

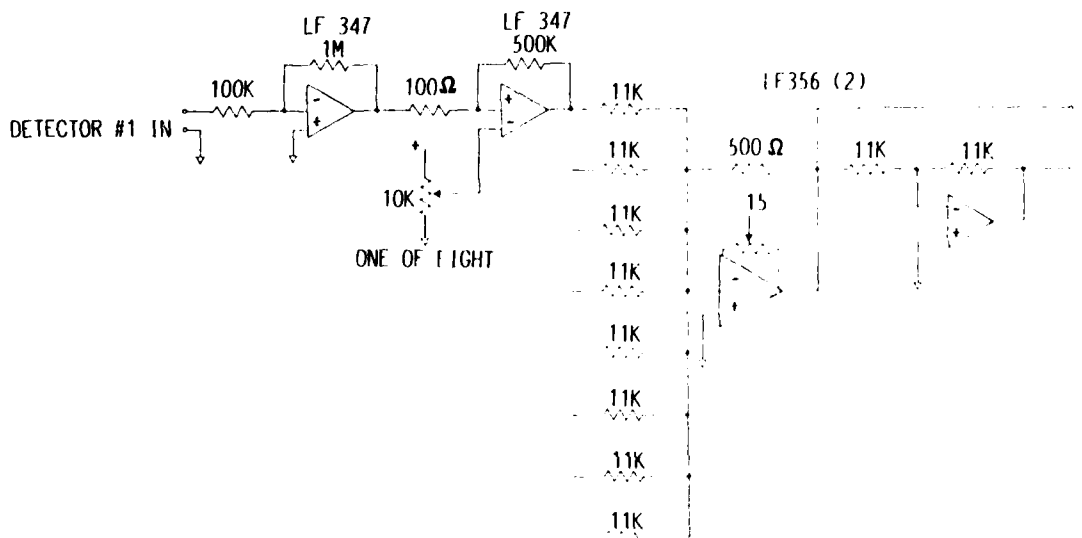


Figure 15. Eight-Element Circuit Prototype. The limited number of elements reduced the capture range and precision of the system.

2.3.3 Servoperformance

Since the photodiode array was only one-dimensional rather than two-dimensional, errors in the mean position of the strand profile occurred if the profile changed. This problem was alleviated by igniting the surface at the short side of the profile (strands were cut at 45° angle) and by using a special, nonsmoking, nonflaking inhibitor that matched the propellant burning rate.²²

Due to a time lag produced by the slide and its motor, the system went into oscillation if the performance specifications were made too tight. The error signal was used as the main drive signal and the instantaneous position was used to estimate an appropriate damping factor for the drive signal. The thresholds for the diodes were adjustable, as were various other circuit parameters. The system was optimized for burning rates between 0.3 and 1.5 cm/s.

The velocity of the surface could not be used as a third input signal, because the limited number of diodes in the array led to a heavily digitized velocity reference signal. The servocircuit was subject to rf pickup from the pulsed copper-vapor laser used in the photography experiment. The ground on the servologic circuit was improved and rf pickup was reduced to 50 mV. Difficulties arose with the range of control of the servopositioner as the chamber pressure was increased. Subsequent to extensive testing, it was determined that although the servosystem could benefit from improved optics and more elements in the diode array, the most serious problem was with the motor controller and the slide--particularly the slide, which had too much friction. Additional improvement in performance resulted from reducing the weight of the slide bar.

Focusing film was put into the camera and the image of the strand surface was observed during test burns. Repeatedly the

surface receded from view even though a scope trace indicated that the servocircuit was holding the strand surface in position. It is believed that the strand flame forms a thermal lens which deflects the servolight beam upwards slightly. This effect would vary from burn to burn, but it apparently increases as the surface moves further from the laser beam. The effect is small and is only troublesome when very tight tolerances are required. Three corrective measures can be applied to the problem. The first is spatial filtering in the collection optics, since the dc component of the servosignal should be the least sensitive to a schlieren effect. The second is the use of an incoherent servobeam, with a large convergence angle. An attempt was made to apply spatial filtering and incoherent optics to the servo-system, but it was found that due to the limitations of the one-inch servoport sufficient signal strength was impossible. Using two-inch servoport it should be possible to make use of optics to spoil the coherence of the servolaser beam without significantly reducing the beam power. The third measure is injection of the pressurizing gas through a tube surrounding the lower end of the strand, to control the flame profile.

2.3.4 Local Burning Rate

The mean, time-averaged burning rate is usually not a fully satisfactory parameter with which to specify a propellant in a motor design. Practical propellants have a dynamic response to the chamber flow.^{8,30-32} An important example is the response of the burning rate to small-amplitude pressure oscillations. This acoustic response can have a critical bearing on the stability of a rocket motor. The acoustic response includes information in the chamber pressure; that is, it contains phase as well as amplitude information, and is a complex quantity. Ideally, both the real and the imaginary parts of this response function are desired.

Although the mean burning rates of propellants are reasonably well known, no quantitative means is used to measure the local instantaneous burning rate. This is unfortunate, as the latter parameter is the one of greatest importance in dynamic phenomena. Traditionally, acoustic response functions have been measured using specially configured burners known as T burners and L burners which are expensive to operate and difficult to calibrate.³³⁻³⁶ The information obtained from them is indirect, has poor resolution, and suffers from a high degree of uncertainty. These burners provide little input on the imaginary part of the response function. Moreover, traditional measures of the acoustic response function have been global measurements. A technique which measures the response on a granular level should be of superior use in understanding the factors responsible for a propellant's oscillatory response. This would entail a study of the local regression of a propellant and its time dependence in the presence of a strong pressure oscillation of known frequency. Both the phases and modulus of the oscillatory regression rate in relation to the acoustic pressure oscillations would be desired.

We have developed and demonstrated a quantitative system for measuring the burning rate along a given line on the surface. This capability is a spin-off from our servopositioning development work. The diode-array output of the servocircuit gives a record of the position of the strand surface where it intersects the servolaser beam. We have shown that this record can be used to track the motion of the surface (See Figure 16). Essentially, this experiment is a back-lit system with a photoelectric detector in place of film. The data may be used without attempting to control the strand position, greatly simplifying the required circuitry. The 31-element linear array used in our system could be extended. More elements in a linear array would provide more detailed information over a long time period. A two-dimensional array would give information on the correlation of local burning rates at different positions.

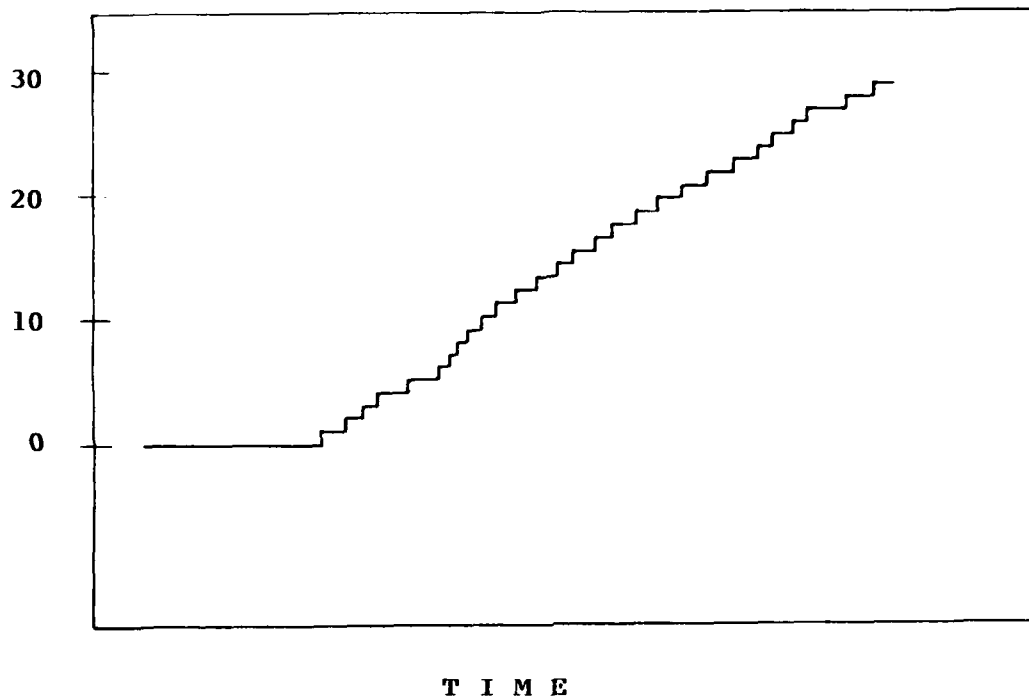


Figure 16. Photodiode Array Trace Showing Surface Location vs. Time.

The data obtained in this manner does not reach the ideal objective of a fully localized burning rate, i.e., approximately "point" information. Rather, it yields an integral of the burning rate along the line formed by the path of the laser beam. However, this rate is certainly far more localized than a rate obtained by integrating the burning rate over the entire surface area. Even more localization can be obtained by burning strands that are peaked at their centers. Above all, this method yields an instantaneous burning rate, which is of the greater interest since it is at least partially localized.

2.4 LASER DEVELOPMENT AND SYNCHRONIZATION ELECTRONICS

The experiment would not be possible without the development of a novel circuit for synchronizing the pulses of the laser to the framing rate of the camera. This circuit and various improvements made on the laser itself are described in the following paragraph.

2.4.1 Pulse Synchronization Circuit

An electric circuit was built to provide a trigger pulse in synchronization with the motion of the high-speed camera whose velocity was not constant, i. e., the camera was accelerating (Figure 17).³⁷ It also provided an automatic transfer from a mode in which the trigger pulses occurred at a constant rate to one in which they were synchronized with the motion of the non-uniformly moving camera. The copper-vapor laser was heated (and heat was essential to its function) by the electrical discharges in the pulsed operation of the laser itself. The laser was designed to run at an average repetition rate of 5000 pulses per second. Unfortunately, the high-speed camera used in the photography did not have a consistent velocity. Therefore, if the pulsing of the laser were not synchronized with the framing rate of the camera the pictures taken would not have been matched to the center of the frame on the camera. Consequently, they would be impossible to interpret when a movie was played back. Therefore, it was

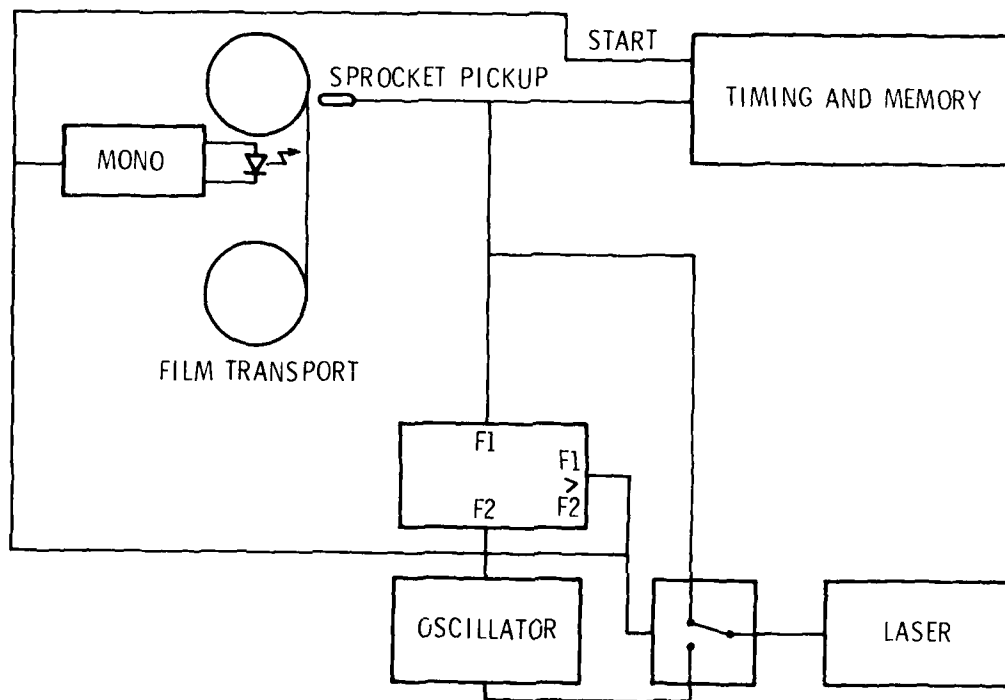


Figure 17. Pulse Synchronization Block Diagram.
 This circuit automatically switches the laser pulse rate from a free-running value to one which matches the camera framing rate.

necessary to synchronize the pulsing of the laser with the framing rate of the camera. It is to this end that the pulse synchronization circuit was developed.

The synchronization of a light source and a camera has been done routinely with a high-speed xenon flash. This can be done for a single flash or for repetitive flashes. Due to significant differences in their mode of operation, synchronization of the high-speed camera with the copper-vapor laser presented a serious problem. The copper-vapor laser was self heated by the electric discharge. The laser was started and warmed up on a free-running oscillator. The high-speed camera frames at an accelerating rate. When the high-speed camera's framing rate was up to this speed, the laser was driven from the camera. At the end of the film, the camera was shut down and the laser was switched back to the free-running oscillator.

The frequency at which the laser was switched over to the camera was determined by the free-running oscillator frequency. When the camera framing rate was equal to the oscillator frequency, the circuit skipped one camera pulse and switched to the camera. This was necessary to prevent the thyatron-triggering circuit in the laser from being double pulsed, causing it to latch up and stop lasing. While the laser was being triggered from the camera, the oscillator frequency was shifted down by about 200 Hz. This hysteresis prevented the circuit from switching between the camera and oscillator due to small changes in the camera speed. When the camera ran out of film, the reverse operation occurred and the laser switched back to the oscillator.

The timing pulses to the synchronization circuit were obtained from a magnetic pickup transducer located in the camera that sensed the proximity of the sprockets that wound the film. Timing marker pulses were made on the film via an LED and fiber

optics. The phase relation was adjusted between the location of the film sprocket holes during runs and the firing of the laser by adjusting a mount for the magnetic pickup transducer in a trial-and-error procedure. Due to its close proximity to the camera motors, inductive noise pickup from motor transients was severe. Consequently, a grounding rod was installed and noise from the laser and its power supply was substantially reduced. The installation contributed greatly to the improved performance of the synchronizing circuit, which subsequently worked satisfactorily.

2.4.2 Copper-Vapor Laser Development

Several copper-vapor lasers have been designed and built at UDRI. An early version of a commercial laser was used for high-speed combustion photography. Since this was really an experimental version of the product, it was necessary to make a number of improvements to the unit. The laser power supply and the head were modified to minimize the possibility of damage due to failure in the cooling system. The Tygon water lines have been replaced with nylon lines, allowing for a higher temperature and pressure margin, and a temperature-sensing interlock has been installed in the power supply. Improvements in various grounds and insulators have resulted in a reduction in the frequency of occurrence of laser lockup and stray timing marks. The laser head has been subject to frequent high-voltage breakdowns. Part of this is an r.f. breakdown, due to the intense fields generated in the 100 MW breakdown discharges in the plasma tube. The fundamental frequency of this r.f. field is about 30 MHz. The laser head is too small, making it difficult to isolate electrically the various components crowded within it. A recommendation was made to the laser manufacturer that they increase the size of their chassis for the laser head. They agreed, and have since increased it to 10 and 16 inches in height and width in their newer units.

In the course of this work, we made the following recommendations, all of which have been adopted by the manufacturer:

- Replacement of the Buna-n "O" rings with Viton "O" rings;
- Antireflection coating of the windows;
- Strengthening of the insulating spacers in the laser head;
- Shock-mounting of the components in the power supply;
- Strengthening of the internal connections in the power supply;
- Changing the location of the gas and vacuum valves in the laser heads to reduce hazards during turn-on and shut-down.

As expected with a new product, there have been several maintenance problems with the copper-vapor laser. A fault in the thyatron driving frequency circuit caused fuses and components to blow. In succession, a transformer, a resistor/diode chain, and a driver tube blew in the driver circuit. A large capacitor in the laser head leaked oil and exploded when the oil reached ground, spraying glass and oil around the laser head. A lead to the bleeder resistor in the head was never properly secured during installation. The lead broke free, producing a short, which set afire some oil remaining from the leakage of the main capacitors. The mylar insulation being used then caught fire and burned out the wiring around the thyatron. It was necessary to remachine the mounts for the capacitors, install capacitors which were resistant to leaking oil, rewire and replumb the laser head, and replace the mylar insulation with pyrex and fiberglass insulation. Unfortunately, the repair was very time consuming, especially as there is no wiring diagram for the laser head, and many of the wires to be replaced had burned through.

The high voltage from the water-cooled cathode and thyatron in the laser head was carried through an extensive portion of the water lines due to the finite conductivity of the water. These

lines were very close to the grounded chassis, and shorts between the chassis and the water line produced leaks in the water line inside the laser head. The conductivity of the water was traced to iron in the heat-exchanger bonnets, so the bonnets were replaced with bronze bonnets, and more electrical insulation was added in the laser head. This greatly reduced the frequency of shorts in the laser head.

2.5 ANCILLARY WORK

The film processing and inhibitor development associated with this effort are described in this section.

2.5.1 Film Processing

Films were processed in-house to provide for good quality control in film development and excellent turnaround time, as well as some overall cost savings. A Cramer 805 processor, which can develop both 16- and 35-mm film, was used, although only 16-mm films were taken. Extensive maintenance is needed to keep this processor running properly.

A variety of films and developers were used depending on the desirability of contrast versus resolution in a given movie. A few general comments can be made about these films. Coarse-grain films require less light for exposure, and yield a high-contrast product. High-contrast films have good visual clarity, which is readily discernable by the viewer, and they project well in a motion picture projector. However, the MTF of large-grain films is poor, and fine details at unity magnification are lost with such films. Moreover, it is difficult to discriminate against flame brightness with these highly sensitive films. Better immunity to flame brightness and an improved MTF can be obtained using fine-grained films.

The resolution of a given type of film is related to the grain size of the film. Fine-grain films yield a high resolution, but are slow, i.e., they require more light exposure for a

given level of development. The resolution limit of a film is given by the number of line pairs per mm that can be resolved. The greater the number of line pairs/mm, the better the resolution of a given type of film. In theory, a film with a resolution of 100 line pairs/mm can discern, or resolve, a $5\mu\text{m}$ object at unity magnification. In practice, the actual resolution will be significantly poorer than this, due to a reduced contrast of the object that is photographed (see paragraph 2.2.1).

Kodak RAR 2496 film with a resolution of 50 line pairs/mm ($10\mu\text{m}$ resolution) and RAR 2479 film with a resolution of 100 line pairs/mm ($5\mu\text{m}$ resolution) with D-19 developer, shellburst 2476 film with 160 line pairs/mm resolution ($3\mu\text{m}$ resolution) using both D-19 developer and D-76 developer, and Technical Pan 2415 film with 400 line pairs/mm resolution ($1.2\mu\text{m}$ resolution) and D-76 developer were used. The resolution of these films was reduced by about a factor of three for low-contrast subjects. Movies made with the RAR 2479 film gave a pleasing visual clarity and $25\mu\text{m}$ resolution at unity magnification. The shellburst 2476 with 200 line pairs/mm resolution was our standard film. It was used at both unity magnifications using D-19 developer and 2X demagnification using D-76 developer. Discrimination against the flames of aluminized propellants at pressures above 200 psi was obtained using Technical Pan film and D-76 developer. The film processing at UDRI is superior to that of professional developers to whom film was sent on trial. All movies made were negatives.

Detail was not good in commercial positive reproductions of our movies, since the vendor who made the positive films used a coarse-grained, high-contrast film. Kodak Technical Pan film was used to make enlargements. Experiments were made with a wide matrix of f stops and exposure times. The developer and enlarging lenses were also varied. It was concluded that HC110 dilution F at 68°F is the best developer for detailed enlargements using Technical Pan film. However, high detail, low-contrast (soft) originals do not reproduce well with standard

equipment. In fact, the high-contrast, low-resolution film used in the initial check-out experiments has given the best enlargements.

2.5.2 Inhibitor Development

A smokeless inhibitor was developed with a burning rate that matched that of the propellant.²² Although this inhibitor may well have potential for use in rocket motors using smokeless propellants, its most immediate application is in strand experiments in pressure bombs in which smoking and flaking are undesirable. Strand experiments using a servopositioner are difficult to perform without a suitable inhibitor. If the inhibitor burns too rapidly, the strand profile will convert to a cone and most of the surface will be below the correct height. In particular, in photographic experiments most of the surface will be out of focus. If it burns too slowly, and leaves large flakes in its residue, it will interfere with the servopositioning beam. If it smokes, the smoke will tend to mask both the servobeam and any optics that may be used in the experiment.

The solid rocket propellant has a natural tendency to burn along all free surfaces and consequently a strand forms a pointed surface during deflagration. Because of the limits in the photographic equipment, the desired burning surface for the experiments was a completely flat plane, parallel with the camera lens, but at an angle with respect to the length of the strand. Unfortunately, untreated propellant will immediately burn on all freely exposed surfaces. This is referred to as "flashing." Flashing produces a pointed surface, unsuitable for these experiments. The relative effectiveness of a number of traditional inhibitors was studied. One common method of inhibition currently being used in strand experiments is simply to leach the propellant with water. If leaching is done directly before deflagration, the water does inhibit burning down the sides of

the strand to a relatively high degree. However, if the water is applied more than a few minutes before deflagration, its inhibitive properties are reduced greatly. Therefore it would not be applicable to any experiments where the propellant needs to be prepared long before deflagration is initiated. Also, water does not have the capability of forcing the propellant to burn at a specific angle due to different coating thickness on different sides of the propellant. Silicone grease did not fully prevent the sides from burning. In addition, it released considerable smoke. The thickness of application of the grease did not affect its performance. Sodium silicate left too much residue, or char. A number of other commonly available materials, including lacquer and teflon, were tested with unsatisfactory results (See Figure 18).

Testing of alternative inhibitors has shown that a phenol formaldehyde polymer works very well as an inhibitor on propellant strands, provided that it is properly prepared with an appropriate solvent. This phenol-formaldehyde polymer is in a partially reacted, thermo-plastic state (Figure 19). It is applied to all free surfaces of the solid rocket propellant, excluding the desired burning surface. The polymer will prevent the deflagration process from spreading to all free surfaces on the propellant, achieving greater control over the burning propellant. If the concentration of the inhibitor layer is correct and the inhibitor thickness is in an appropriate range, the polymer will also burn away at the same rate as the propellant. In this case, there is no shell formation or intrusive residue left behind.

Once the polymer was established as having the most promising performance, further tests were performed to optimize the application procedure. The optimum concentration for the inhibitor coating of phenol in acetone depends on the operating pressure. An example of results for low-pressure operation is shown in Figure 20. It is expected that the optimum concentration will

INHIBITION

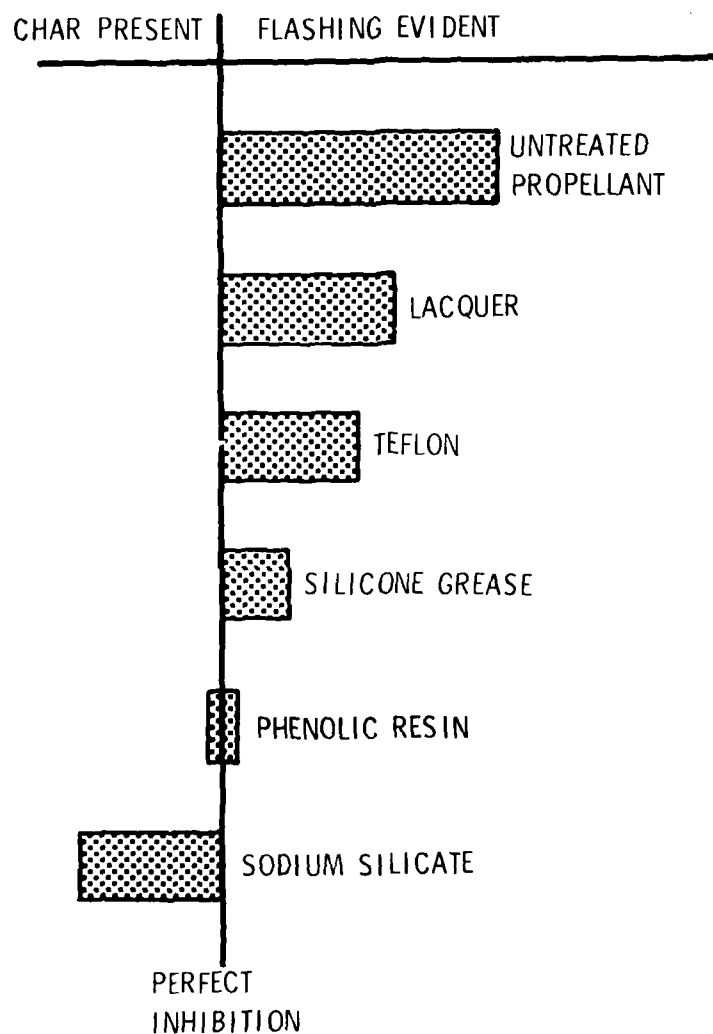


Figure 18. Qualitative Performance of Commonly Used Inhibitors for Strand Experiments.

CROSSLINKED PHENOLIC RESIN

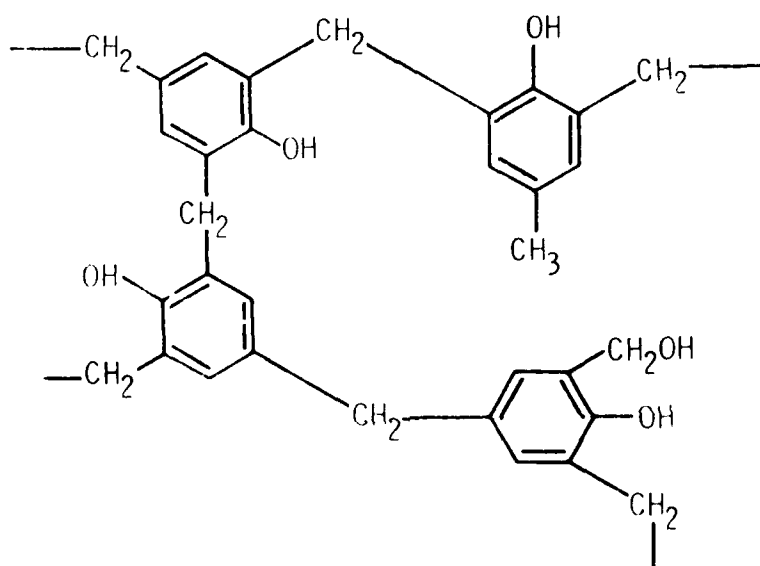


Figure 19. Chemical Structure of Phenolic Resin Copolymer Unit.

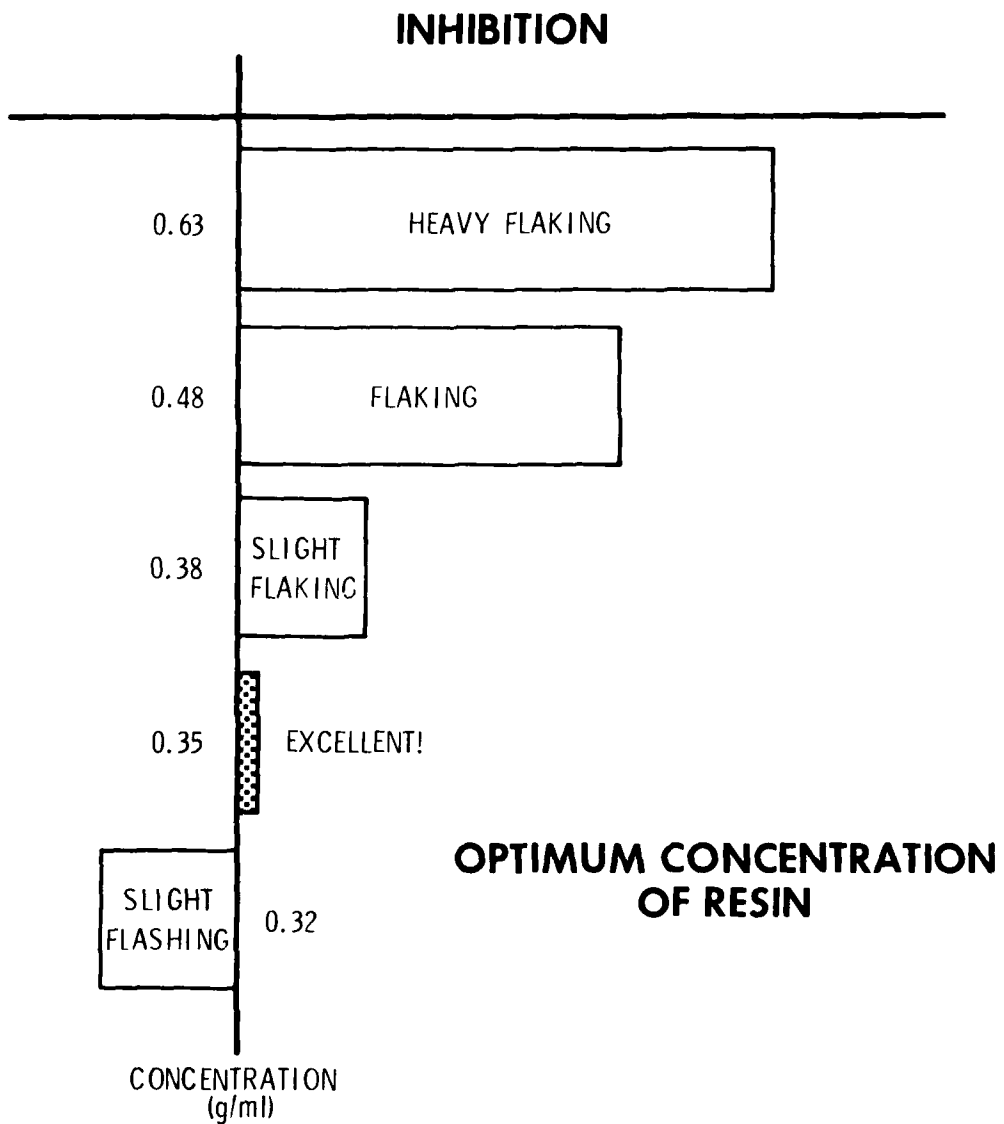


Figure 20. Qualitative Behavior of Polymer Inhibitor vs. Solution Concentration.

be different for propellants of varying formulation. Experiments were also undertaken to find the most appropriate solvent; acetone yielded a product with the most consistent results. Tests with 1000 weight polyethelene glycol (PEG) as an additive showed that more than 0.2 g/ml of PEG added to the phenol solution will cause flaking.

The initial results obtained with this inhibitor are very encouraging, but further work is needed to obtain a no-smoke, no-flake product of general interest in the solid-propellant combustion community. Additives are needed to increase the burning rate to match high-regression-rate conditions. Work should also be done to improve quality control, which is primarily limited by long (6-hr) drying times. Quality control could be improved with oven drying; both conventional and microwave ovens are possibilities for this process. A vat should be designed to control the length of the coating application time. This quality assurance would aid the progress of both research-level strand experiments and any widespread use in the solid propellant community. Additives are needed to increase the flexibility of the coating. Possibilities for enhancing flexibility are clean-burning cellulose fibers, or various rubber-based compounds. The present formulation was developed for work at low (50-200 psi) pressures. Formulations for work at higher (300-1000 psi) pressures can easily be developed.

2.6 OPTICAL CORRELATOR

Much of the quantitative data needed for a statistical description of propellant combustion can be expressed in terms of correlation functions and probability density functions. This requires the automatic processing and analysis of a large number of frame sequences. It also requires high-quality films of excellent resolution and a thorough characterization of the propellants and the burn conditions.

For years motion pictures have been extremely useful for obtaining information about the motion and behavior of a field such as the flowfields in a wind tunnel or the behavior of a turbulent flame in a combustion process. However, these movies have, for the most part, been limited to providing the qualitative understanding of the phenomena under study. Because a single picture is so rich in detailed information, reduction of the data in a movie tends to overwhelm the capacity of the digital computer. Therefore, there has long been an unmet need for a means of reducing images of essentially quasi-random fields to quantitative data.

We have demonstrated that the required automated statistical data analysis is possible using optical data processing.³⁸ A successful application of this technique demands images that comprise a large number ($> 10^6$) of pixels. In the case of propellant deflagration this implies 6mm x 6mm areas of the burning strand surface. This specification is due to the need to accumulate sufficient statistics, the desirability of determining long-range correlations, if any, and the logic of obtaining a realistic environment for the particles under study. The above considerations indicate that movies of the leading edge of a flame and/or of a limited field-of-view are unsatisfactory; a large field-of-view looking through the flame is desired.

A simple optical correlator has been built, demonstrated, and proven useful in addressing the above needs. This instrument has provided hard quantitative data to support our qualitative observations.

2.6.1 Concept

Among the types of sophisticated functions used to reduce partially random variables commonly in use are correlation functions and power or spectral density functions. The device described here provides a good quantitative description of the

correlation function of a field. The advantages of the optical correlator system are that it is economical and very fast, especially in the data reduction of photographs or movies. It gives both auto- and cross-correlation, in terms of both location and time. With a simple computer algorithm auto- and cross-power spectral data densities can be obtained from the correlation functions. The correlator is a simple analog system which uses a series of lenses to perform optical operations on transparencies of the images to be processed. In short, it is a single-purpose analog device which has the advantages of speed and parallel processing, as well as economy.

No viable means of obtaining quantitative data from movies of the deflagration of surfaces such as solid rocket propellant has been known to exist. Some digital computer systems have been developed for the analysis of pictures. However, because digital systems must process data serially, and because they can only handle digital data, they are slow and essentially inappropriate for the task in question. In particular, these machines must first transfer the analog information provided on the film to a detailed store of digital information. The amount of detail in a single picture is vast; it can easily incorporate a million pixels, so the memory store for thousands of frames from a motion picture is indeed enormous. To obtain a simple linear transform integral, such as the correlation distance between points, we may have to perform 10^8 or more operations.

Image analysis can be accomplished by digital data processing. A digital approach requires point-by-point analog-to-digital conversion and serial operations. To analyze a frame from a movie, we must convert the light output we get from a photograph into digital numbers, store them, and then repeat this process at least a million times to cover the entire frame. This requires sophisticated hardware equipment to perform the A/D conversion, and a large computer memory for data storage. In addition, software is required to control the serial operations

and perform simple integrals. Consequently a digital approach is a prohibitive operation.³⁹

For the above reasons, an alternative approach, analog optical data processing, was selected. It must be emphasized that optical data processing examines an entire image at once, i.e., it has the capability of performing parallel data processing. This stems from the ability to map simultaneously a single two-dimensional data field onto a second field. It is important to note that such an optical system has two spatial degrees of freedom, in contrast with a digital system whose single independent variable is time. An optical system also has good speed potential; the simultaneous analog multiplications take place as fast as the response time of the photodetector. In summary, optical data processing systems are powerful, fast, and economical.⁴⁰

The simplest way to perform an incoherent optical operation is to make use of the ability of a lens to form images.⁴¹ The principle of this processing is straightforward. If a transparency with transmittance $f(x,y)$ is imaged onto another transparency with transmittance $h(x,y)$, the resultant transmitted intensity is the product of the two transmittances, i.e., $f(x,y)h(x,y)$. If a collection lens and a photodetector integrate the resultant intensity product, an output of the form

$$I = \iint f(x,y)h(x,y)dx dy \quad (11)$$

is obtained.

This operation can be approached by two techniques. In the first technique, a lens images the uniform incoherent source into two transparencies which are in contact. The intensity product formed by the two transparencies is integrated by the second lens and a photodetector; the output is given by Equation (11).⁴² This technique has a mechanical difficulty if one of the two transparencies is moved because of the direct contact between the

two transparencies. Therefore, it is more convenient to separate them (Figure 21).

Many one-dimensional and two-dimensional linear transformations can be achieved by moving the first transparency, the second transparency, the imaging lens, or any combination of those. These include convolutions, correlations, power spectra, filtering, and other useful linear transformations. In spatial scanning systems the integration takes place over spatial variables, as seen in Equation (11). When the second transparency is translated by an amount of x_0 , the photodetector output yields a one-dimensional cross-correlation of the form⁴¹

$$I(x_0) = \int f(x)h(x_0 - x)dx . \quad (12)$$

2.6.2 Practical Considerations and Limitations

It is essential to ensure that all the optical components, including the light source, lenses, and photodetector are centered on the optical axis. This minimizes off-axis aberrations and vignetting. The first transparency must be illuminated uniformly. Because of the problem in uniformly illuminating the first transparency within the translating distance, the first transparency was fixed at the most uniformly illuminated spot, and the second transparency was moved.

The most difficult problem was aligning the image of the first transparency on the second one, due to the nature of the propellant image. The shape of the propellant during combustion does not have straight edges or clear corners that can be used for alignment. A three-axis system was used for image alignment. The z-axis translation stage fixed the magnification obtained from the imaging lens. Two translation stages gave the x-y translation portions. The third stage rotated the transparency in the x-y plane. The use of these three stages eased the image

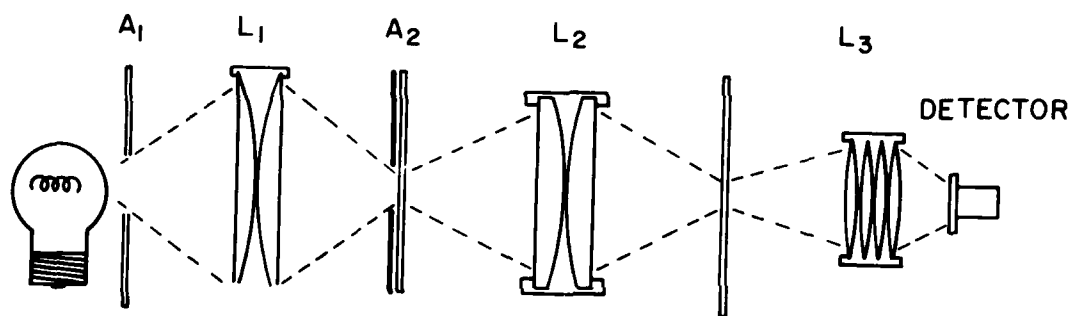


Figure 21. Optical Correlator. This simple layout provides parallel data processing and integration. Apertures are designated by A, lenses by L, and transparencies by T.

alignment. Final alignment required judgment on the part of the experimenter.

Because the transparency darkness was not the same across the image of the propellant strand, a condition of maximum output light did not necessarily indicate that the two transparencies were properly aligned. Minimizing background effects required a dark background and several bright features.

Results were significantly affected by the contrast of the transparency. Work began with a fine-grain positive film transparency (Figure 22). This type of film has a continuous range of opacity and the resultant data were difficult to interpret (Figure 23). Therefore, films were processed by using a very high contrast film, resulting in pure black and white tones (Figure 24). This type of positive film enhanced the signal from the bright intermediate-sized features in the images. Sharp correlation functions were obtained from these photographs. We interpreted the widths of these correlation functions as a direct measure of the sizes of bright features on the surface (Figure 25).

Electronic noise from the dual power supply (± 15 V) and from the active elements of the circuit itself was minimized. The power supply noise was reduced by coupling the high-voltage leads of the power supply to the ground lead with two capacitors, one for the positive lead, and one for the negative lead. The circuit noise was reduced by shunting a capacitor across the feedback resistor.

2.7 STEREO CINEPHOTOGRAPHY

Present understanding of the details of propellant combustion is sparse and would benefit from more detailed qualitative information, as well as quantitative information. More information is

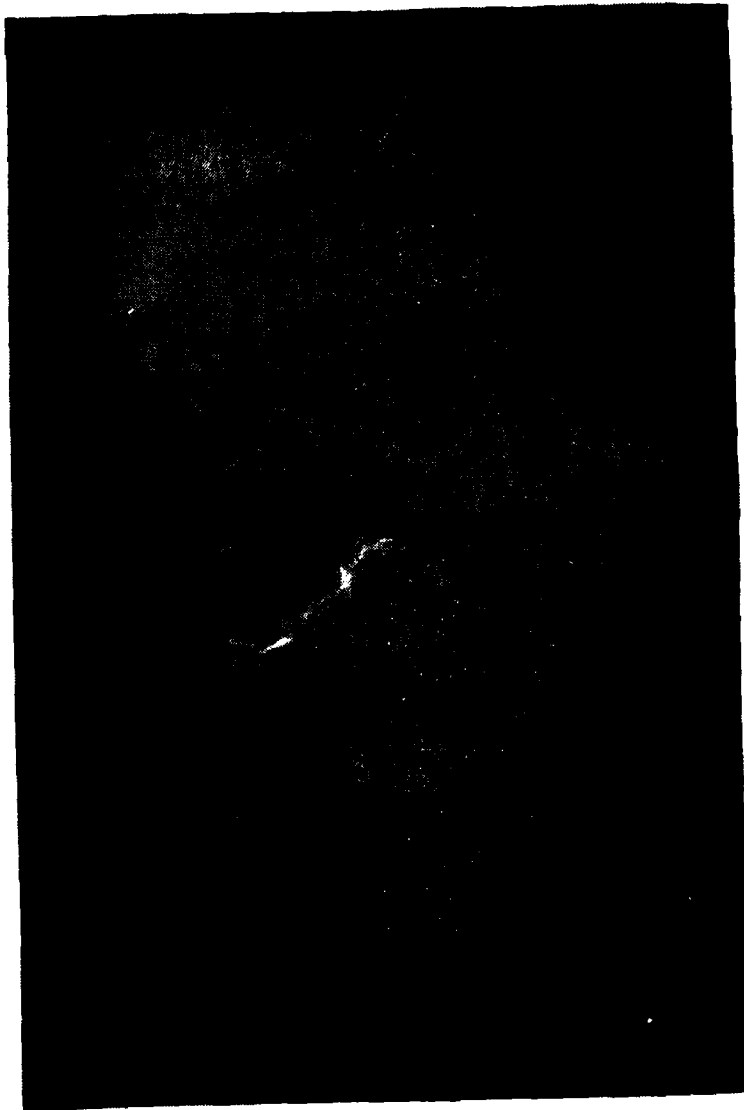


Figure 22. Untreated Photograph of Combusting Surface. The lack of contrast on the surface impairs the signal-to-noise ratio.

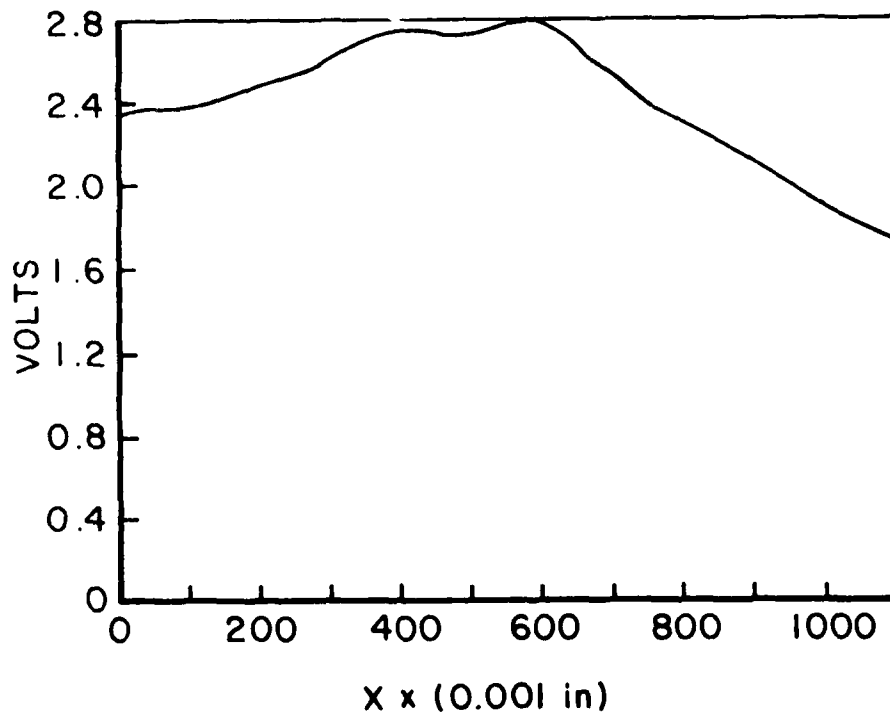


Figure 23. Correlation Function Obtained from Untreated Photograph. Long-range correlations are difficult to extract without analyzing a large number of frames.

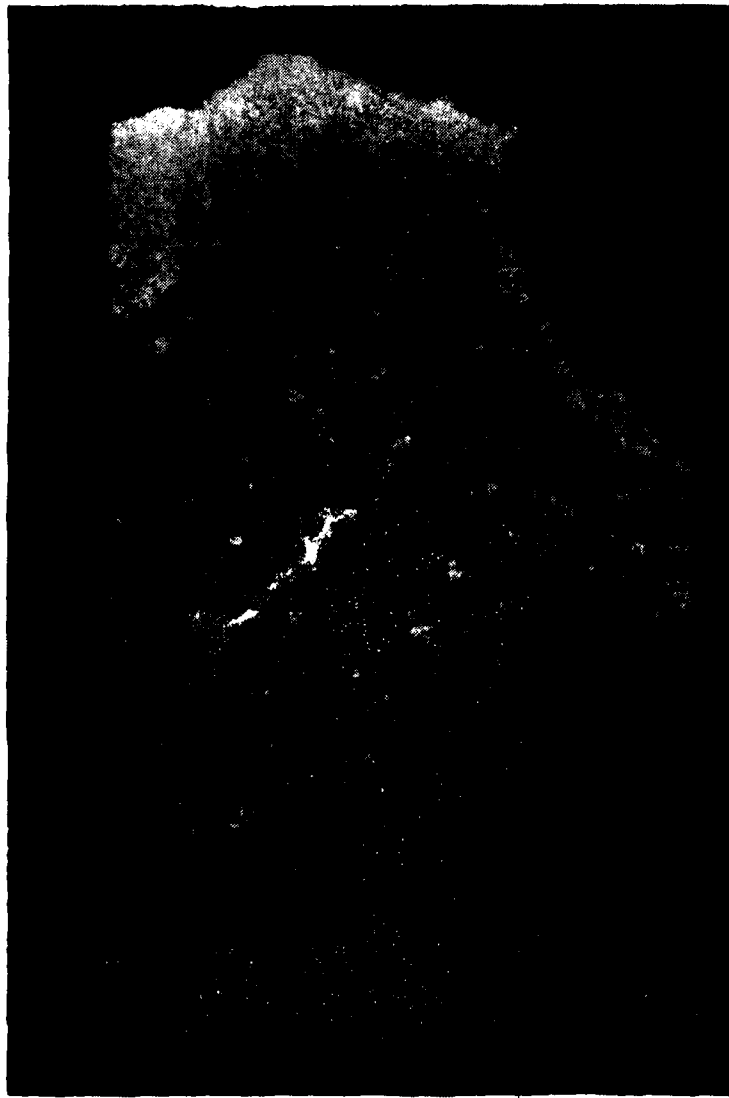


Figure 24. High-Contrast Photograph of Combusting Surface. High-contrast processing enabled us to obtain a signal dominated by the brightest features on the surface.

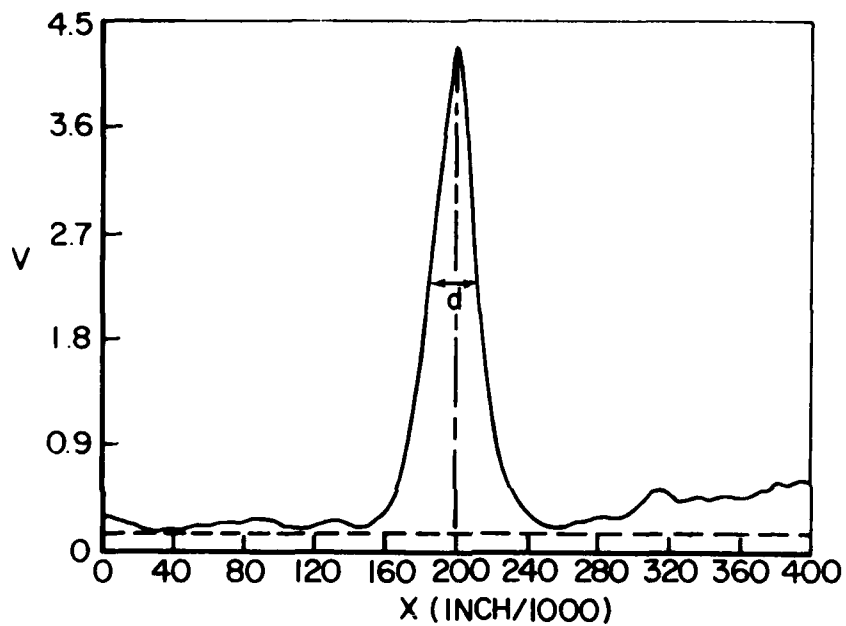


Figure 25. Correlation Function Obtained from a High-Contrast Photograph. We interpret the width of the correlation peak as a measure of the size of the bright features on the surface.

needed about localized transient burning rates, their dependence on grain and binder composition and grain size distribution, and the coupling of regression rates of the various constituents in the propellant. High-speed movies have long been a very useful means of obtaining a qualitative understanding of the behavior of combusting surfaces, especially in the field of solid propellant combustion. It may be possible to analyze a series of high-speed cinematic frames to trace the local regression of the surface along trajectories normal to the local surface and not simply to record the recession of a mean plane normal to the strand axis. This objective requires movies with depth perception. One means of achieving depth perception is by stereo cinephotography.

Detailed front-lit stereo movies of the combustion of solid propellants have been made.⁴³ It is believed that these are the first stereo movies ever made on solid-propellant combustion. Two complementary images of good quality at pressures up to 250 psi were obtained. Stereo movies at 300 and 350 psi were also made. At 350 psi problems were encountered from one camera angle with flame turbulence, although we were able to obtain pictures in focus at 300 and 350 psi.

The two viewing ports were configured at a wide (90°) angle to maximize the depth resolution obtainable (Figure 26). This resulted in dramatic differences in the viewing perspective. Our motivation for selecting a widely disparate viewing angle was to maximize our depth resolution. The relation between the depth resolution, ξ_d , of a stereo movie and the transverse resolution, ξ_T , of the optical system is given by

$$\xi_d = \xi_T / \sin \frac{1}{2} \phi$$

where ϕ is the angle between the two viewing ports. Since an ability to discern depth relationships is limited by the depth resolution, it is helpful to make ξ_d as small as possible.

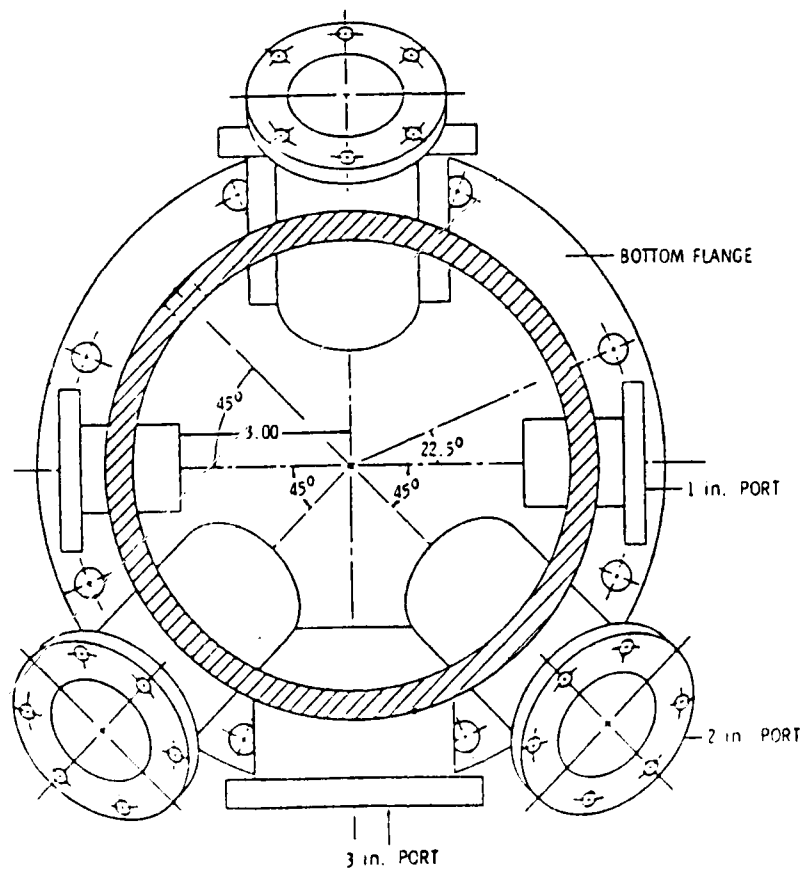


Figure 26. Top View of Port Design for Window Bomb. The 90° angular separation of viewing ports maximized potential depth of resolution.

Consequently, with cinephotography optics of a given quality, good depth resolution can only be achieved by using a large angle between the two viewing perspectives. The objective in seeking good depth resolution was to optimize scientific understanding. A narrower stereo perspective would be more suitable for obtaining films with images that could be superimposed by an appropriately configured projector to lend a natural image to the viewer. This was not the aim of the experiment. However, since stereo feasibility with a wide viewing angle has been demonstrated, it is felt that stereo movies using a narrow viewing angle can easily be obtained.

The camera and the stereo camera optics were mounted on a single 30-in.-x-18-in.-x-0.5-in. (75-cm-x-45-cm-x-1.3-cm) aluminum plate. Brackets were made to secure this plate to a camera tripod at the desired height and angle. Mirrors directed the light from each of the two viewing ports to a second set of mirrors, which then directed the (by now) nearly parallel light beams to a single camera lens (Figure 27).

The viewing ports were arranged at a 45° angle with respect to the horizontal so that they looked down on the deflagrating surface of a vertically mounted strand (Figure 28). The illuminating light was brought in along a horizontal path, and the strand surface was cut at 45° to face the viewing ports as much as possible.²¹ The detailed movies obtained were immune to flame brightness and motion blur over a wide field-of-view at 7000 frames per second.³⁷

Our initial trials of stereo photography were troubled by differences in optical path length, vignetting between the two optical trains, and vibrations induced by the camera. The first two difficulties were overcome by very careful alignment. Vibrations were minimized by damping and clamping. The area of support contacts to the mounting plate was increased and the

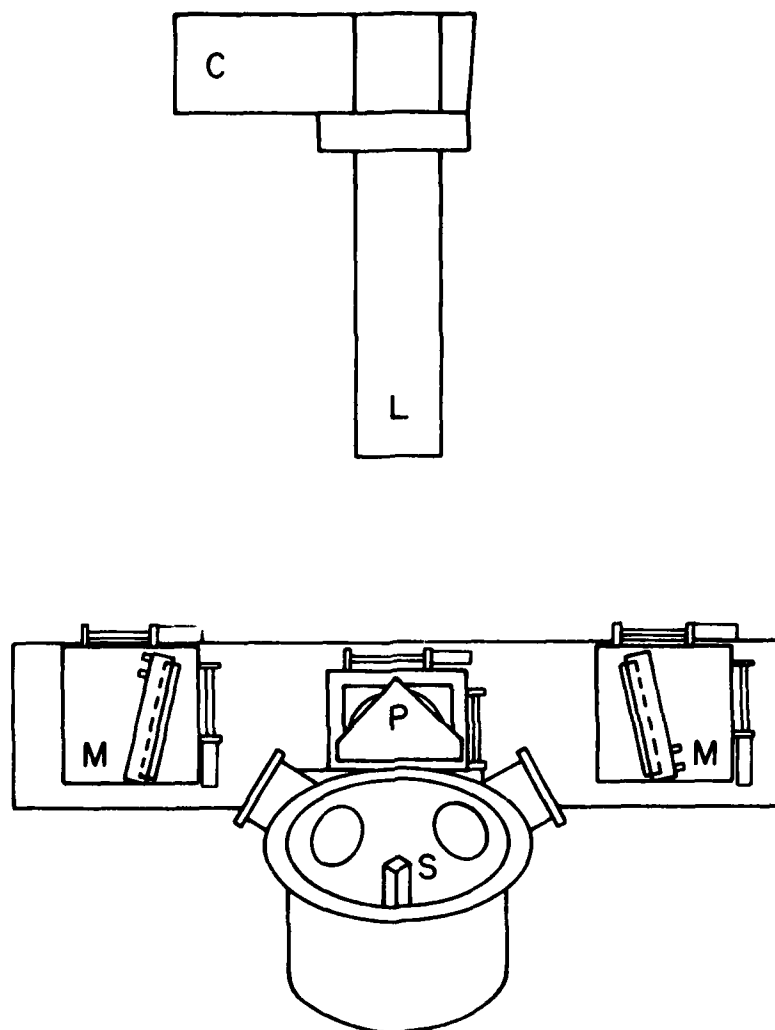


Figure 27. Stereo Optics. A mirror and prism arrangement allowed us to simultaneously record two separate images.

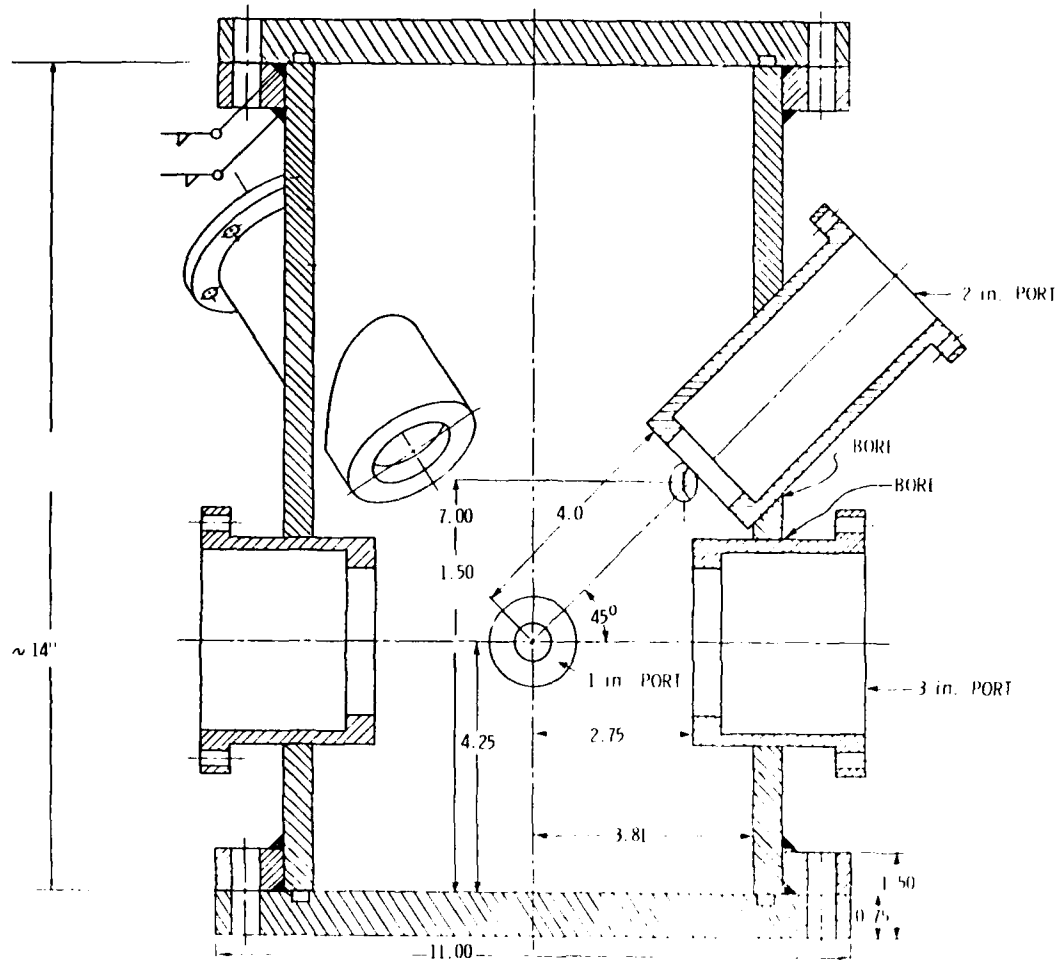


Figure 28. Side View of Window Bomb. The 45° viewing angle allowed us to survey the entire active surface of the strand.

mounting plate was tightly clamped to the camera framework. The mounts for the mirrors and prism were secured with wedges and clamps. The camera lens was also clamped. A half-inch-thick layer of damping material was placed under the camera and the rail supporting the stereo optics. The prism directing the two images to the camera was reconfigured to an 85° angle instead of a 90° angle. This provided more flexibility in positioning the mirrors, and allowed us to locate them so as to minimize vibrations. The different perspectives of the sides of the strand were oriented in such a way that they crossed at an odd angle, resulting in what was effectively a double exposure of the strand sides with the strand surfaces. This problem was surmounted by crossing the images from the left to the right. Thus the recorded pictures are mirror images of the true object field.

A sample stereo image is shown in Figure 29. The groove in the strand face shown in this figure was cut to provide good thermal contact for the ignition wire. This groove has widened due to deflagration. The differing textures on the strand face mark the flame front. Note that no flame emission or motion blur appears in these photographs; single frames are not fuzzed out, despite a low-contrast object field. The change in perspective in the two images in Figure 29 is dramatic. Figures 30 and 31 show a similar strand, taken several frames apart during the course of filming. A close inspection of these photographs will reveal changes in the surface topography between the two frames, and a sharply varying perspective between the left and right images of a given particle.

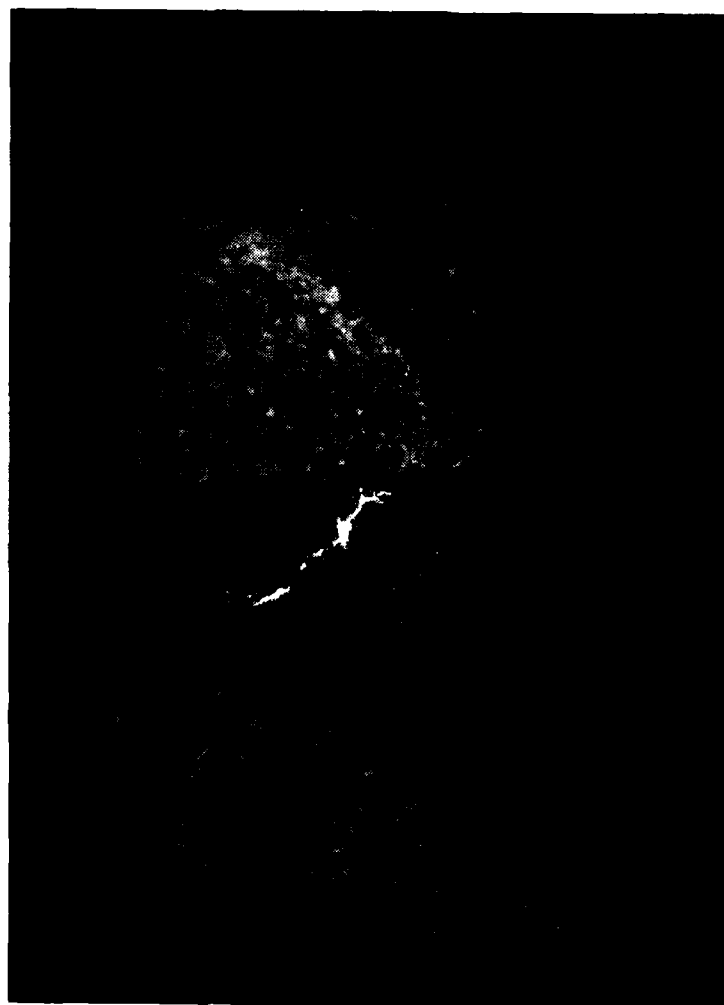


Figure 29. Stereo Images of Burning Propellant Surface. No fuzziness occurs due to flame brightness, motion blur, or flame turbulence.



Figure 30. Stereo Images of Burning Propellant Surface. Surface has not yet fully ignited.



Figure 1. Stages Evolution of Crystalline Subject as Shown
in Figure 29, Taken Several Frames
Later. The surface is now fully
imbedded.

SECTION III

RESULTS

The experiment was successful in accomplishing most of its goals. A window bomb with plentiful optical access suitable for the experiment was designed and built. A servopositioning circuit based on an array of photodetectors was designed and demonstrated. Movies were taken on ten AP propellants at pressures of 100, 200, and 500 psi. Stereo cinephotography was demonstrated. The results from this work are described below.

3.1 GENERAL PERFORMANCE

The 1.4 mJ pulse energy and 510 nm monochromatic output of the copper-vapor laser in conjunction with slow (insensitive) film and a line filter permitted flame brightness to be overcome and the surface topography within the combustion region to be seen through the flame. The intensity of the laser pulses together with their short (25 ns) pulse width allow use of the laser pulse as a shutter. Conventional cinephotography uses shutters that are tied to the film framing rate. Consequently the motion blur induced by the movement of the film in the camera is a fixed fraction of the frame size. For a 16-mm film with a 1/100th shutter at unity magnification this implies a minimum blur of 70 μm . A 25-ns pulse width produced a film blur of only 1 μm , even at a framing rate of 6000 frames/s. The copper-vapor laser, slow film, and line filter have been totally successful at overcoming flame brightness and motion blur; these two technical difficulties have no bearing on the quality of the films.

The movies clearly prove the ability of the pulsed laser technique to overcome difficulties associated with the inherent incandescence of the flames of individual particles and of motion blur, particularly blur produced by the motion of the film in the camera. A highly logical approach was pursued by the use of an

intense, high-energy, monochromatic, and extremely short laser pulse. Difficulties with flame brightness and motion blur simply do not occur. It is emphasized that these front-lit movies are taken across the entire field of the burning strand and that an ability to reach framing rates of six to seven kilohertz has already been demonstrated. Although this makes the cinephotography task difficult, these requirements are essential to understanding the response of the propellant to external high-frequency driving forces such as pressure oscillations and to finding correlations in the behavior of various particles across the surface in the presence of pressure oscillations. Furthermore, these movies were made for extended time periods. Great effort went into making movies which will obtain high resolution for a great many frames. In general, useful information during the entire course of a movie can be obtained. Resolution on the order of 25 microns is obtained, even on propellants which contain no metal. This is an especially difficult task because such propellants have no inherent contrasts on their surfaces. Furthermore, these movies are seldom troubled by smoke from the burning propellant, even in movies on carbonized and heavily aluminized propellants. It is demonstrated that speckle due to the coherence of the light source can easily be eliminated, and good ruggedness against flame turbulence has been shown.

The above performance should be put in proper context with conventional technology. Although experiments using conventional illumination have in some instances matched any one of the above performance characteristics of these movies, it is not known that anyone has been able to achieve comparable results when all of these various performance parameters are taken together: field-of-view, duration of the movie, framing rate, and resolution, not to mention immunity to flame brightness, smoke, and the ability to resolve details on low-contrast surfaces.

3.2 AP MATRIX BEHAVIOR

A large number of movies (200) on various solid propellants, all of which have ammonium perchlorate (AP) formulation, were taken. Most of the movies were made on wide-distribution AP propellants. The particle sizes are in various proportions of 3/20/400 microns. These propellants are 87% AP and 13% HTPB binder, using both IPDI and DDI curatives. All of the movies were taken at low (15-500 psi) pressures.

At low (<500 psi) pressures the burning surfaces of wide-distribution AP propellants are soft or molten, in sharp contrast to the highly featured unignited material at the edge of a flame. These smooth surfaces have a low albedo. Detailed movies of ignition of wide-distribution propellants were made and in these movies the course of a burn as it proceeds across the surface of a strand can be followed. These movies show clearly the transition from the rough, detailed surface of the unburnt propellant to the smooth field of the burnt propellant.

The large 400- μ m particles have a generally low albedo that nearly matches that of the inhibitor. Localized (50-200 μ m) features of high albedo stand out sharply on the large particles. Indeed, the localized features offer such a strong contrast to the background of fully deflagrating surfaces that their association with the large particles is not readily apparent. From one to three such features are found on each of the large particles. Usually there is one feature, generally located at the tip of the large particle. These features are probably raised bumps or protuberances on the large particles whose orientation is such as to reflect light toward the camera preferentially.

In the ignition studies large areas of the large particles have high albedos prior to ignition, but once inside the flame front these high-contrast areas immediately shrink down to the

size seen on all fully burning surfaces. The time scale for this metamorphosis is less than 1 ms. Often they split into two or three bright spots. As new particles emerge at the surface, the bright features appear at the reduced size. As indicated in Figure 32, the mean size of these bumps is a strong function of the operating pressure. This mean size is uncorrelated with the initial formulation of the propellant.

The most striking aspect of these movies is that the above bright features appear to oscillate just above or at the surface of the burning propellants. These oscillations generally are of large amplitude and occur at frequencies on the order of several hundred hertz to a kilohertz in the absence of any forcing pressure oscillations. They are very distinctly a phenomenon associated with the burning of the propellants. Occasionally, some evidence of an isolated particle going through an oscillation on surfaces that are as yet unburnt can be seen. However, the oscillation phenomenon is very definitely a ubiquitous occurrence on all burning surfaces. In particular, on the ignition studies it can clearly be seen, in the same frames in which there is a portion of the propellant burning and a portion not burning, the sharp transition to surfaces in which there is widespread oscillation of these particles upon ignition. These ignition films prove that the observed oscillations are not experimental artifacts. Much of the apparent oscillation is due to localized flame turbulence, which, due to a random lensing action, can change the perceived location of various features at the surface. This occurs without blur due to the short pulse width of the laser. Since large features at the surface do not appear to oscillate, it is not clear whether the raised features themselves actually oscillate, or whether the perceived oscillation is entirely due to flame turbulence.

A new phenomenon is observed when pressure is increased in the vicinity of 200 psi. At this pressure, tufts or plumes of dark materials are seen rising from the surface. These plumes

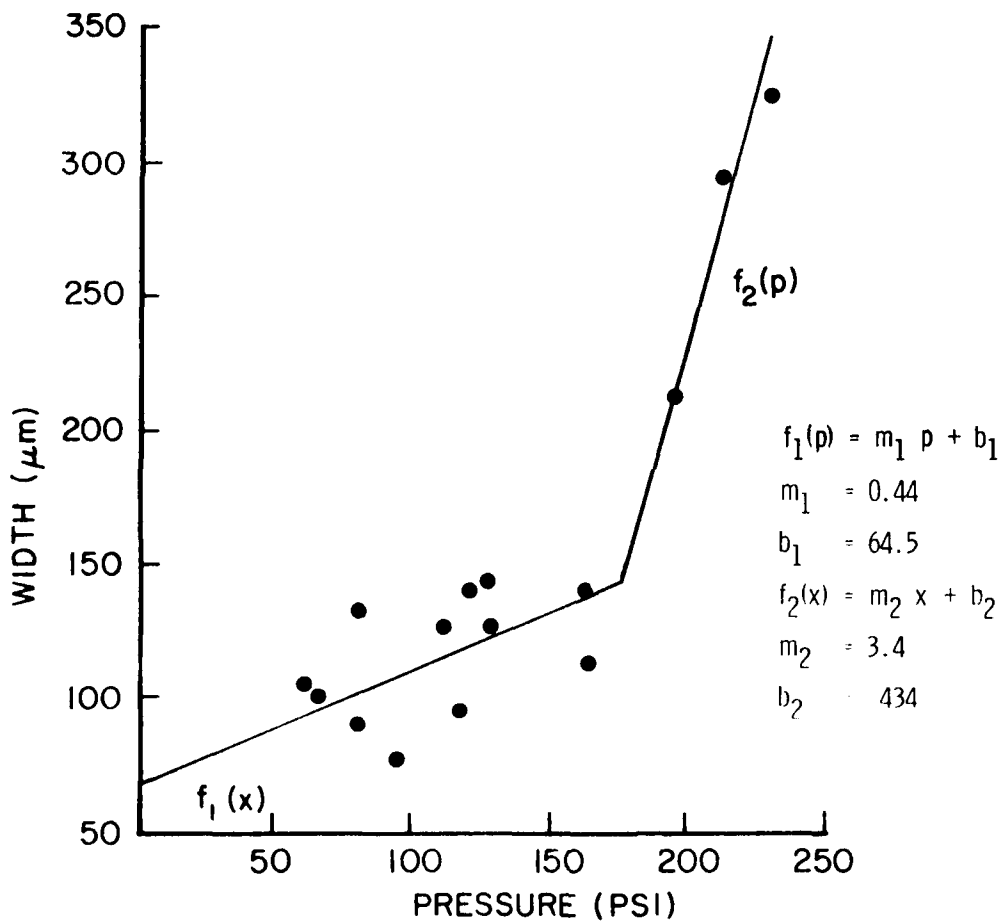


Figure 32. Best Fit to Correlation-Width Data. The break in the line implies a change in physical behavior at 150 psi.

are not seen at lower pressures, and they are quite localized. The plumes also oscillate or wave in the manner of flags and are presumably driven by turbulence in the gas evolving from the surface. Occasionally the plumes will break off from the surface. Their identity is currently undetermined, but it is probable that they are in fact smoke.

It is confirmed that the 400-micron diameter particles do not stand up strongly from the surface, that is, they are for the most part buried or suppressed at the level of the general smooth surface. At low pressure, the contours are well defined. This phenomenon has been observed previously.

3.3 CORRELATOR RESULTS

Our optical correlator was used to analyze selected frames from the movies. Fifteen different movie frames were analyzed at different pressures (See Table 1). It was found that the characteristic sizes of bright features at the surface vary with pressure but not with the particle mix of the propellant. A best fit to the data was made using three different curves and a standard χ^2 routine.⁴⁴ The first curve was an exponential function in the form

$$f(p) = A + B e^{p/c}. \quad (13)$$

The parameters giving the best fit to the data were $A = 59.27$, $B = 15.87$, and $C = 90.97$ (Figure 33). The reduced χ^2 was 0.43, indicating a 96% probability that the data were nonrandom.

The second curve was a quadratic function in the form

$$f(p) = A + Bp + Cp^2. \quad (14)$$

A χ^2 fit yielded the following optimized parameters: $A = 70.0$, $B = 0.12$, and $C = 2.46 \times 10^{-3}$ (Figure 34). The reduced χ^2 of 0.47 gave a 94% probability that the data were nonrandom.

TABLE 1.
 SIZE OF BRIGHT FEATURES VERSUS OPERATING PRESSURE.

Pressure (PSI)	Propellant		Width μ m	Film #	Frame #
	Grain #	Large grain %			
62	7	38	104	LS93	28849
63	15	47	102	R12	35840
80	7	38	92	R19	35568
80	7	38	134	R19	35546
95	12	38	78	LS90	70060
112	17	44	128	R24	78090
116	10	47	97	R25	75736
121	11	50	142	R23	90363
127	13	41	145	LS62	27396
127	17	44	128	LS63	90472
163	15	47	115	R26	70811
164	9	44	142	R27	76607
195	12	38	215	LS34	83599
211	11	50	205	LS35	73826
228	9	44	326	R29	97390

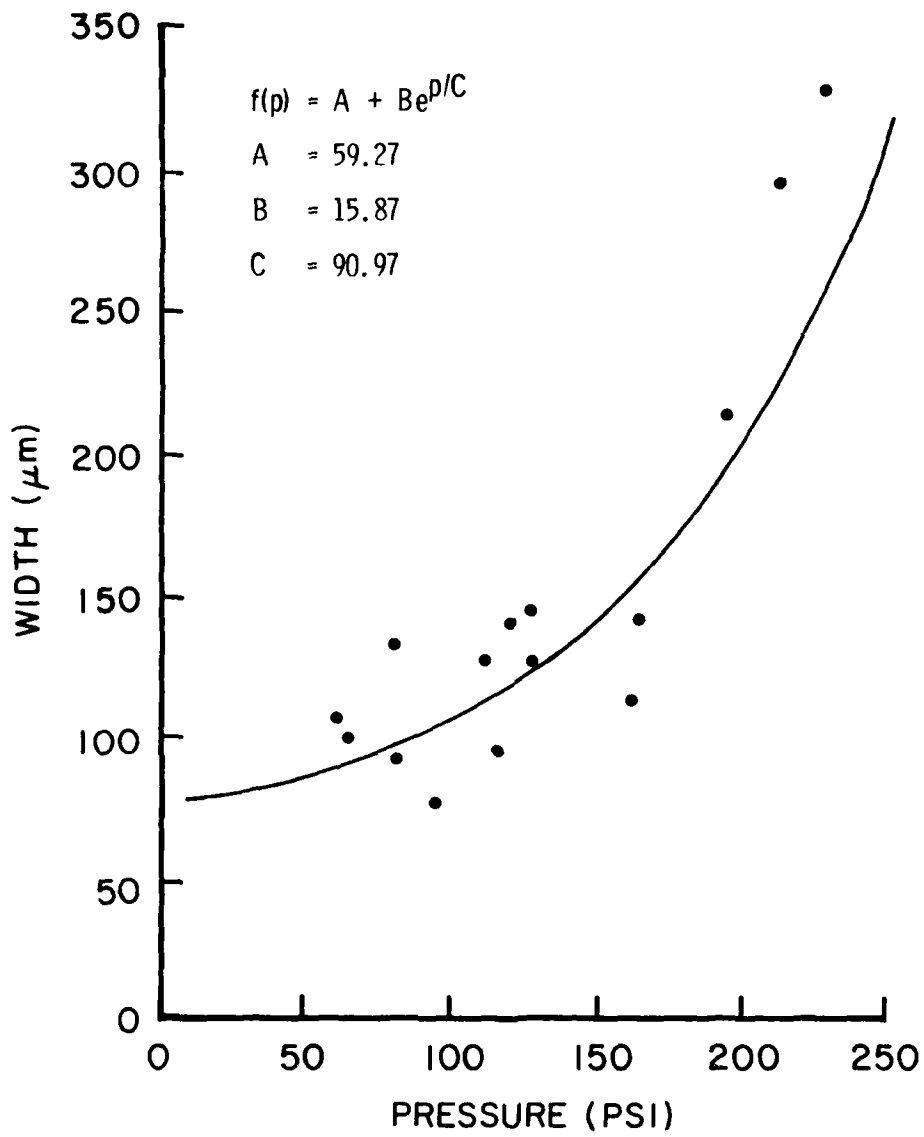


Figure 33. Exponential Fit to Size Versus Pressure Data.

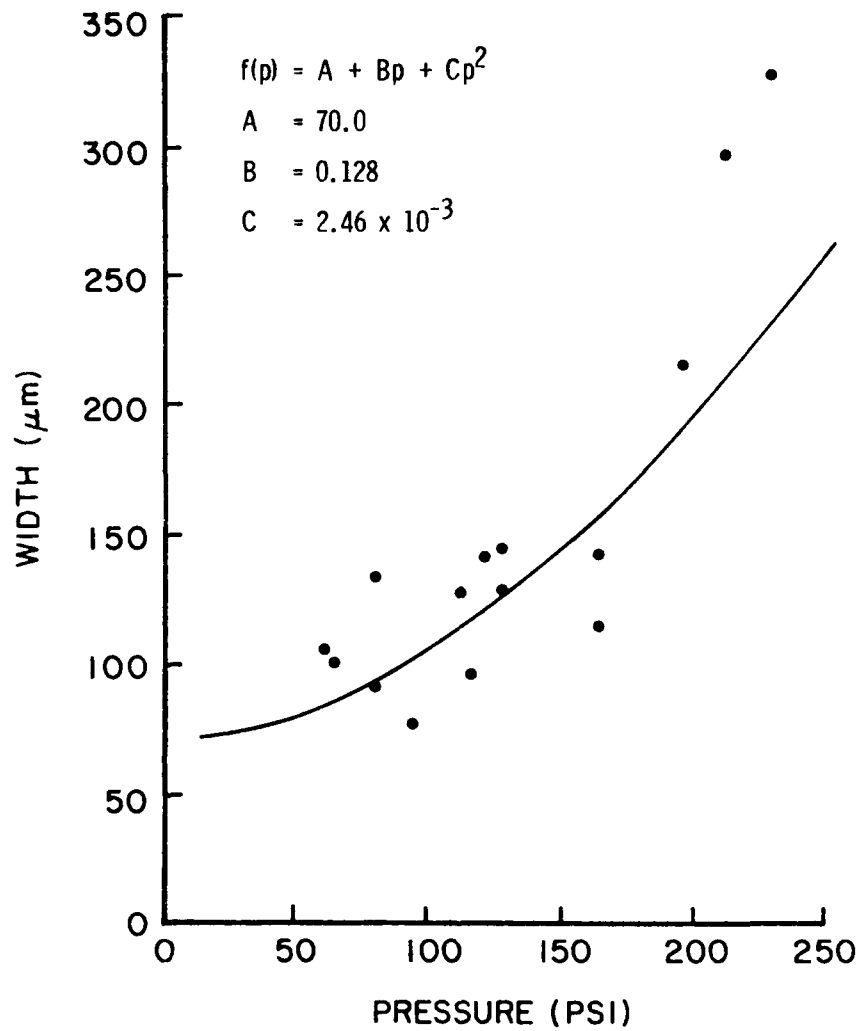


Figure 34. Quadratic Fit to Size Versus Pressure Data.

The third curve was a broken line of the form $f_1(p)$ and $f_2(p)$, where

$$f_1(p) = m_1 p + b_1 \quad (15)$$

and

$$f_2(p) = m_2 p + b_2 \quad (16)$$

In Equations (15) and (16), m_1 and m_2 are respectively the slope for the first line and the second line, b_1 is the y-intercept of $f_1(x)$, and b_2 is the y-intercept of $f_2(x)$. A χ^2 fit gave $m_1 = 0.44$, $b_1 = 64.5$, $m_2 = 3.4$, and $b_2 = 434$ (Figure 32). The reduced χ^2 of 0.36 indicated a 98% probability that the data were non-random. The conclusion is that the best fit for the data set is given by the broken line.

One frame in a movie was compared with succeeding frames to obtain the temporal as well as the spatial correlation. The plot of the highest response of each frame versus the frame-time order was also expected to be in the shape of an exponential decay. This would result from the decrease in the size of particles as they burned. The measured curve turned out to be a damped cosine function (Figure 35). This implies that an oscillation is associated with the combustion process. These data are the first quantitative verification of this result. To make the best curve fit for these data points, a standard χ^2 fitting routine was again used. The specified function to which we fit the data points was a damped cosine curve:

$$f(t) = A[B + \cos \omega t] e^{-\nu t}, \quad (17)$$

where A was the initial peak amplitude, B gave a dc offset to the oscillation amplitude, ω was the oscillation frequency, and ν was

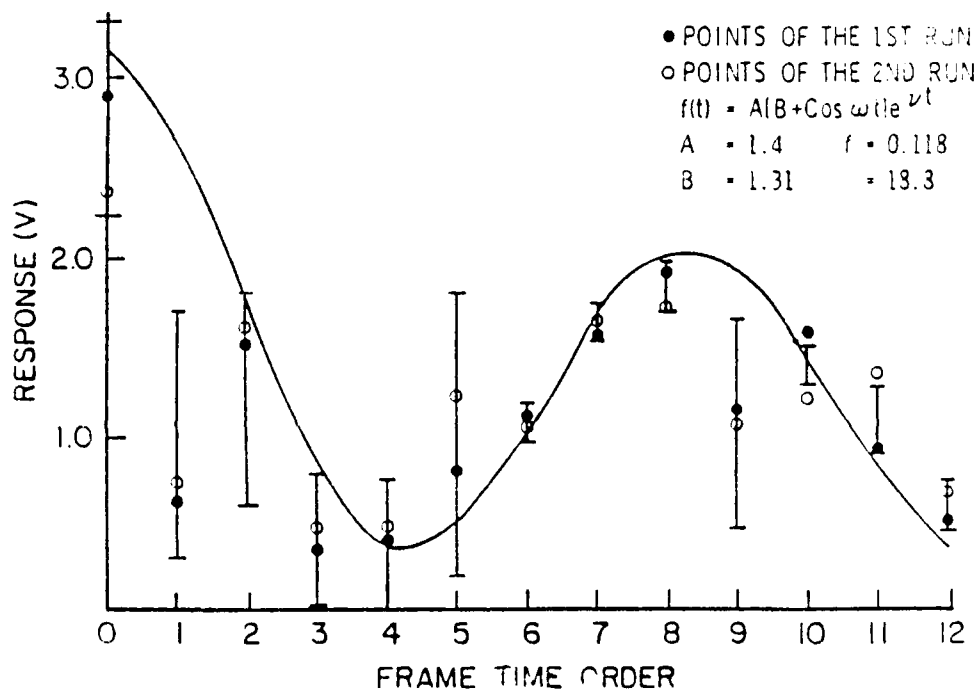


Figure 35. Time Dependence of Correlation Peak Height. The apparent correlation width depends on the frame number in a given sequence. The trend shows a damped cosine dependence with time.

the damping rate. The optimized parameters were: $A = 1.4$, $B = 1.31$, $F = 0.118$, and $v = 18.8$. A reduced χ^2 of 0.38 was also obtained, giving a 97% probability that the data were nonrandom.

A similar analysis was used to measure the trend in the widths of the correlation functions vs time (Figure 36). Although there is a good deal of scatter in these data, it does appear that the widths of the cross-correlation functions increase as the time between frames increases. This suggests movement in the apparent location of the bright features at the surface. A standard linear-regression routine was used to obtain a fit. This routine made a least-square fit to the data with a straight line, i.e.,

$$f(t) = mt + b, \quad (18)$$

where m was the slope, and b was the y -intercept of the fitted line. With different weightings for the various y -values represented by the bars on the plot, the routine's output was $m = 4.68$ and $b = 126.8$. The linear correlation coefficient was 0.74. The probability that the data points were not correlated was 0.4%.

3.4 ADDITIONAL OBSERVATIONS

Movies were undertaken without using the line filter on the camera optics to explore the possibility of examining particle ignition. With shellburst film, streaks from flames occurred across the frames, but it was not possible to associate them with a given particle. Due to flame brightness, most of these films were of unacceptable quality. These streaks did not occur at low pressure using the slower Technical Pan film. It was even possible to film aluminized propellants (e.g., ANB 3066) successfully without a line filter at pressures below 100 psi using this film. Some control on the amount of flame emission

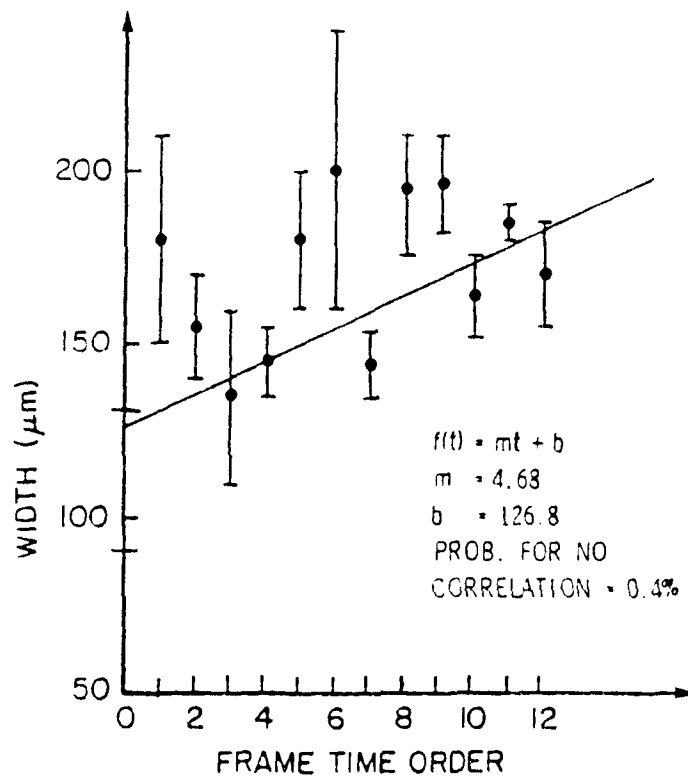


Figure 36. Width of Cross-Correlation Function vs. Separation in Time. Frames from the same sequence in a movie, taken at different times, when compared.

AD-A169 300

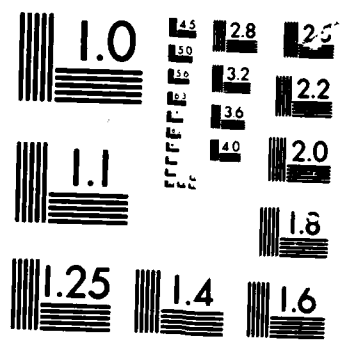
PULSED-LASER HIGH SPEED PHOTOGRAPHY OF ROCKET
PROPELLANT SURFACE DEFLAGRATION(U) DAYTON UNIV OH
RESEARCH INST R J BECKER MAY 86 UD-TR-85-147
AFRPL-TR-86-039 F04611-83-K-0023

2/2

UNCLASSIFIED

F/G 21/9.2 NL





MICROCOPY

CHART

recorded could be achieved by varying the line width of the line filter and the speed of the film.

In many cases, although the end of strand was out of focus, good sequences of the performance of the inhibitor were obtained. The melting and bubbling of inhibitors and the smoking and/or flaking of some inhibitors showed clearly. So, as a side effect, the studies show that copper-vapor laser illumination gives good information on inhibitor performance. Small adjustments were made in the scattering geometry to achieve as much shadowing by particles as possible. There was not much that could be done if the incoming laser beam did not strike the surface at an oblique angle. This would require either cutting strands with square ends or reconfiguring the window bomb. The angle at which the laser beam or camera was oriented with respect to the windows could not be moved by very much, due to the limited size of the ports and the increase in reflections if normal incidence was not used. If the strands were not cut at a 45° angle, the depth-of-field problem over most of the field-of-view would be accentuated.

SECTION IV

CONCLUSIONS

The utility of copper-vapor laser illumination for high-resolution, high-speed cinephotography of solid-propellant deflagration has been demonstrated. Movies can be made with a ratio of the field dimension to the smallest resolvable size of greater than 300. These movies are unimpaired by flame brightness, motion blur, or laser speckle.

The performance of the experiment is critically dependent on the combined Modulation Transfer Function of the camera lens and film. Since the depth-of-field and resolution are coupled, high resolution exacts a penalty of a severely limited depth-of-field.

The use of white-light illumination prior to this program has placed severe constraints on the depth-of-field and field-of-view that can be obtained from such films at high resolution. The use of an intense pulsed laser for illumination relaxes these constraints. Consequently, it is now possible to survey an entire strand surface in detail. In this manner, meaningful statistical information can be obtained about particle behavior in the flame. In particular, analyses of interactions between particles and correlated behavior, if any, can be made.

At pressures below 500 psi, high-albedo features appear in a size range (50-200 microns) that does not occur in the original formulation. The widths of bright features vary with pressure, but not with propellant type.

The concept of a photo detector array has been demonstrated to achieve tight position control. Practical limitations are due to the number of diodes in the array and the quality of the motor drive and its controller. The main limitations of this circuit could best be alleviated by adding more elements to the array.

Ultimate performance will be determined by the ability of the optical subsystem to overcome the lensing action of the propellant flame. Possibly this can be achieved with incoherent optics. The signal from the photodetector array gives an excellent record of the instantaneous local burning rate.

Correlator results demonstrate that simple optical systems can yield useful quantitative statistics on movies of random data fields. The existing correlator is difficult to align due to the requirement of an exact overlay between two frames, including successive frames in a movie, which never have exactly the same profile. It is more convenient to work with a high-contrast transparency than with a low-contrast one. Transparencies should be made under the same conditions and with the same exposure time for accurate results.

An inhibitor coating developed for solid propellants does not smoke or flake and can be tailored to match the burning rate of the propellant. The base for this inhibitor is a partially reacted phenolic polymer. This material completes its polymerization upon heating in the combustion process, and subsequently chars. The monomer base comes in powder form. Experiments on $\frac{1}{8}$ -inch strands showed greatly superior performance compared to other materials commonly used in laboratory work.

A trade-off must often be made between detail in a film and visual quality. The MTF of a lens/film system falls off steadily with decreasing feature size. Low-contrast features are most severely affected by this fact, so that small-scale, low-contrast details tend to fuzz out. Large-grain film and a high-contrast developer result in a film with good visual clarity, while a fine-grain film and a soft developer give a more faithful representation of the object field. Similar considerations apply to reproductions, whether by motion picture projectors or enlargements of individual frames. The fine detail obtained in a

soft picture leads to a blurred result in reproductions using standard commercial equipment.

Initial stereo feasibility studies on propellant combustion have been successfully completed. This demonstrates that stereo movies are possible, and problem areas that need improvement to make stereo movies practical have been identified. One such area is customized mirror mounts which need to be designed.

SECTION V

REFERENCES

1. R. L. Glick and R. J. Becker, "Recommended Experiments Related to Difluoramino Propellants," University of Dayton, Dayton, OH, UDR-TR-81-94 (1981).
2. W. B. McLean, "Combustion of Solid Propellants and Low-Frequency Combustion Instability," NOTS TP 4244 (1967).
3. E. S. Sutton, "From Polysulfides to CTPB Binders, A Major Transition in Solid Propellant Binder Chemistry," AIAA Paper No. 84-1236.
4. G. A. Flandro, "A Simple Conceptual Model for the Nonlinear Transient Combustion of a Solid Rocket Propellant," AIAA Paper No. 82-1222.
5. F. A. Williams, M. Barrere, and N. C. Huang, Fundamental Aspects of Solid Propellant Rockets, Technivision Services, Slough, England (1969).
6. F. E. C. Culick, "Acoustic Oscillations in Solid Propellant Rocket Chambers," Astronautica Acta 12 (2) p. 113 (1966).
7. R. S. Brown, A. M. Blackner, P. G. Willoughby, and R. Dunlap, "Coupling Between Velocity Oscillations and Solid Propellant Combustion," Paper No. 34, AFOSR/RPL Chemical Rocket Research Meeting, Lancaster, CA (March 1985).
8. R. Srivastava, "Reaction Boundary Layer Model of Steady and Oscillatory Combustion of Solid Propellants," AIAA Paper No. 85-1110.
9. J. N. Levine and J. D. Baum, "Modeling of Nonlinear Combustion Instability in Solid Propellant Rocket Motors," Nineteenth International Symposium on Combustion, p. 769 (1982). J. D. Baum and J. N. Levine, Nonlinear Combustion Instability in Solid Rocket Motors, University of Dayton, Dayton, OH, UDR-TR-81-158 (1982).
10. R. S. Brown and R. C. Waugh, "Coupling Between Velocity Oscillations and Solid Propellant Combustion," United Technologies Chemical Systems Division Report No. CSD 2749-AR-1.
11. R. R. Miller, "Self-Extinguishment Propellant Development," AFRPL-TR-82-096 (December 1982).

12. L. D. Strand and R. P. McNamara, "A Variable-Frequency Driver-Microwave Transient Regression Rate Measurement System," p. 155 in Ref. 19.
13. L. D. Strand, "Investigation Of Microwave Doppler Shift Measurement System of Solid Propellant Combustion Response Function," AFRPL-TR-83-085 (1984).
14. T. L. Boggs, R. L. Derr, and M. W. Beckstead, "Surface Structure of Ammonium Perchlorate Composite Propellants," AIAA Journal, 8 (2), p. 370 (1969).
15. M. Hanzawa, "A Theoretical Study on Depressurization Induced Extinction of Solid Propellant," AIAA Paper No. 76-635.
16. C. L. Merkle, S. L. Turk, and M. Summerfield, "Extinguishment of Solid Propellants by Depressurization: Effects of Propellants Parameters," AIAA Paper No. 69-176.
17. G. E. Jensen, "An Experimental Study of Solid Propellant Extinguishment by Rapid Depressurization," Technical Report NASA CR-66747 (1969).
18. A. Gony, "Combustion Studies of Metallized Fuels for Solid Fuel Rockets," AIAA Paper No. 85-1177.
19. T. L. Boggs and B. T. Zinn, ed., Experimental Diagnostics in Combustion of Solids, American Institute of Aeronautics and Astronautics (1978).
20. T. L. Boggs, J. E. Crump, K. J. Kraeutle, and D. E. Zurn, "Cinephotomicrography and Scanning Electron Microscopy as Used to Study Solid Propellant Combustion," p. 20 in Ref. 19.
21. J. L. Laird, P. F. Luehrmann, and R. J. Becker, "Application of a Copper-Vapor Laser to High-Speed, High Resolution, Front-Lit Cinephotography of Solid Propellant Deflagration," AIAA Paper No. 85-1257.
22. J. L. Laird and R. J. Becker, "A Novel Smokeless, Non-Flaking Solid Propellant Inhibitor," to be published in the Journal of Propulsion and Power.

23. T. L. Boggs, J. E. Crump, K. J. Kraeutle, and D. E. Zurn, "Cinephotomicrography and Scanning Electron Microscopy as Used to Study Solid Propellant Combustion," p. 20 in Experimental Diagnostics in Combustion of Solids, T. L. Boggs and B. T. Zinn, ed., American Institute of Aeronautics and Astronautics (1978).
24. C. L. Andrews, Optics of the Electromagnetic Spectrum, Prentice Hall, Englewood Cliffs, NJ (1960).
25. Optics Guide 3, Melles Griot, Irvine, CA (1985).
26. E. Hecht and A. Zajac, Optics, Addison-Wesley, Reading, MA (1979).
27. R. J. Becker and J. M. Aulds, "Design and Performance of a Detector Array Servopositioner for Strand Experiments," Submitted to the Journal of Propulsion and Power.
28. R. J. Becker and J. L. Laird, "Optical Consideration in Obtaining a Statistical Data Base on Propellant Deflagration," Presented at JANNAF Combustion Meeting, Pasadena, CA, October 7, 1985.
29. T. Edwards, D. P. Weaver, and R. Adams, "A High-Pressure Combustor for the Spectroscopic Study of Solid Propellant Combustion Chemistry," submitted to Review of Scientific Instruments.
30. F. E. C. Culick, "Acoustic Oscillations in Solid Propellant Rocket Chambers," Astronautica Acta 12 (2) p. 113 (1966).
31. F. E. C. Culick, "A Review of Calculations for Unsteady Burning of a Solid Propellant," AIAA 12 (6) pp. 2241-2254 (1968).
32. N. S. Cohen, "Combustion Response Functions Of Homogeneous Propellants," AIAA-85-1114, AIAA/SAE/ASME/ASEE 21st Joint Propulsion Conference, Monterey, CA (July 1985).
33. J. R. Wilson and M. M. Micci, "Direct Measurement of High Frequency Solid Propellant Pressure Coupled Responses," AIAA Paper No. 85-113.

34. M. W. Beckstead and F. E. C. Culick "A Comparison of Analysis and Experiment for Solid Propellant Combustion Instability," Naval Weapons Center Technical Publication 4531 (1968).
35. "Combustion Tailoring Criteria for Solid Propellants," Lockheed Propulsion Company, AFRPL-TR-69-190 (1969).
36. J. R. Osborn, "Evaluation of Solid Propellant Ballistic Properties," *Combustion and Flame* 20. pp. 193-197 (1973).
37. R. J. Becker, P. F. Luehrmann, J. L. Laird, and J. J. Heinrichs, "Application of a Pulsed Laser to Cinephotography of Deflagration Over Extended Surfaces," Submitted to the *Journal of Propulsion and Power*.
38. R. J. Becker and M. A. Al-Saffar, "A Simple Optical Correlator for the Quantitative Statistical Data Analysis of Photographs of Random Fields," submitted to the *Journal of Propulsion and Power*.
39. W. K. Pratt, Digital Image Processing, Wiley, New York (1978).
40. M. A. Monahan, K. Bromley, and R. P. Bocker, "Incoherent Optical Correlations," *Proc. IEEE* 65, 121 (1977).
41. W. T. Rhodes and A. A. Sawchuk, "Incoherent-Optical Processing." *From Topics in Applied Physics, Vol. 48. Optical Information Processing Fundamentals*, ed. S.H. Lee, Springer-Verlag, New York (1981).
42. J. W. Goodman, Introduction to Fourier Optics, McGraw Hill, New York (1968).
43. R. J. Becker, J. L. Laird, and J. J. Heinrichs, "Front-Lit Stereo Cinephotography of Solid Propellant Combustion," submitted to the *Journal of Propulsion and Power*.
44. Phillip I. Bevington, Data Reduction and Error Analysis for the Physical Sciences, McGraw Hill, New York (1969).

END

DTIC

7-86